Chemistry Research Journal, 2023, 8(2):1-31

Available online www.chemrj.org

Research Article

ISSN: 2455-8990
CODEN(USA): CRJHA5

On the relationship between electronic structure and herbicidal activity of biphenyl ether derivatives having a five-membered heterocycle

J.S. Gómez-Jeria

Quantum Pharmacology Unit, Laboratory of Theoretical Chemistry, Department of Chemistry, Faculty of Sciences, University of Chile. Las Palmeras 3425, Santiago CP 7800003, Chile.
Correspondence to facien03@chile.cl (J.S.G.J.)

Abstract The Klopman-Peradejordi-Gómez (KPG) QSAR method has been employed to search for formal relationships between herbicidal activity and electronic structure in a series of biphenyl ether derivatives having a five-membered heterocycle. Full geometry optimization and electronic structure calculations were performed within the Density Functional Theory at the B3LYP/6-311g(d,p) level with water as solvent (Polarizable Continuum Model). Three statistically significant relationships were found. The results of these three equations are completely compatible with each other. With that information, some drug-PPO interactions have been suggested. We analyzed the conformations of the optimized molecules as well as the conformers of the most and least active molecules. A qualitative analysis of the overlap of the molecules in their optimized form was also carried out for comparison purposes. Finally, the MEPs of the more active molecule were compared with those of the less active molecule at different distances from the nuclei. It is hoped that this information will be helpful to experimentalists. In particular, the conformers of molecule 21 offer an interesting possibility to develop new molecules.

Keywords Klopman-Peradejordi-Gómez method, herbicides, protoporphyrinogen oxidase, QSAR, solvent effects, conformers, common skeleton, molecular electrostatic potential, local atomic reactivity indices

Introduction

Herbicides are substances used to control weeds. Sodium dinitrocresylate ("Sinox"), the first chemical herbicide, was developed in France in 1896. In the late 1940s, new herbicides were developed and the era of weed killers began. The dark side of the use of herbicides and defoliants was in charge of the British and American Empires facing anti-colonial liberation movements. Between 1948 and 1960, the British Empire used herbicides and defoliants in the Malaysian rural area (as well as crop fields) to deprive Malayan National Liberation Army of cover and potential sources of food. The American Empire used herbicides in Southeast Asia during the Vietnam War, officially claiming that herbicidal (and incendiary agents such as napalm) were not chemical weapons. About 10% of the land surface of South Vietnam was sprayed. Almost 85% of the spraying was for defoliation and around 15% was for crop destruction. The policy of destroying the food supply of the civilian population in an area of conflict has been banned under Article 54 of Protocol I of the 1977 Geneva Conventions.

"Since the first case in 1970, confirming the resistance of the common groundsel (*Senecio vulgaris*) against triazine herbicide, the number of resistant weeds against various herbicides has been considerably increasing. To date, more than 200 species have been reported to be resistant to different types of herbicides" [1-3]. One of the targets of

herbicides is the protoporphyrinogen oxidase (PPO) enzyme. PPO catalyzes the oxidation of protoporphyrinogen IX (Protogen) to protoporphyrin IX (Proto) [1]. The three-dimensional structure of plant mitochondrial PPO revealed that this homodimer folds into a compact structure that includes an FAD-binding, a substrate binding, and a membrane-binding domain. The PPO FAD binding domain has structural homologies to other flavoenzymes and it is known to be near the binding site of xenobiotic inhibitors. A number of different herbicides act as competitive inhibitors of PPO, resulting in the cytosolic accumulation of Proto [1]. When exposed to light and O_2, protoporphyrin IX can react with oxygen and generate reactive oxygen specie, which results in the peroxidative destruction of cell membranes and rapid cell death [4, 5].

Numerous groups of chemicals have been synthesized and tested for PPO inhibition [6-17]. Recently, a group of diphenyl ether derivatives containing a five-membered heterocycle were synthesized and tested against PPO inhibition [4].

This article has two objectives. First, to test if the linear form of the KPK method is capable of finding relationships between the electronic structure and the inhibition of the PPO enzyme. If the first objective is met, the second is to provide solid chemical information to experimentalists to design better herbicides.

Selection of molecules and biological activities

The selected molecules are a group of biphenyl ether derivatives and were selected from a recent study [4]. Their general formula and protoporphyrinogen oxidase (PPO) inhibitory activity are shown, respectively, in Fig. 1 and Table 2.

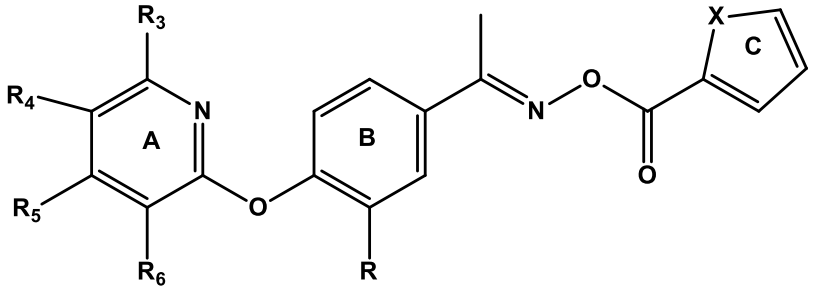

Figure 1: General formula of biphenyl ether derivatives

Table 1: Biphenyl ether derivatives and PPO inhibitory activity

Mol	R_3	R_4	R_5	R_6	R	X	log(IC_{50})
1	CF_3	H	H	H	H	O	0.27
2	H	CF_3	H	H	H	O	-0.14
3	H	H	CF_3	H	H	O	0.11
4	H	H	H	CF_3	H	O	-0.51
5	NO_2	H	H	H	H	O	0.62
6	Me	H	H	H	H	O	0.78
7	H	H	Me	H	H	O	0.76
8	Br	H	H	H	H	O	0.63
9	H	H	Cl	H	H	O	0.54
10	CF_3	H	H	H	H	S	0.32
11	H	CF_3	H	H	H	S	-0.10
12	H	H	CF_3	H	H	S	0.18
13	H	H	H	CF_3	H	S	-0.67
14	Me	H	H	H	H	S	0.85
15	H	H	Me	H	H	S	0.84
16	Br	H	H	H	H	S	0.64
17	H	H	Cl	H	H	S	0.54

18	CF_3	H	H	H	OMe	O	-0.13
19	H	CF_3	H	H	OMe	O	-0.74
20	H	H	CF_3	H	OMe	O	-0.35
21	H	H	H	CF_3	OMe	O	-1.33
22	NO_2	H	H	H	OMe	O	0.57
23	H	H	NO_2	H	OMe	O	0.49
24	CF_3	H	H	H	OMe	S	-0.11
25	H	CF_3	H	H	OMe	S	-0.66
26	H	H	CF_3	H	OMe	S	-0.33
27	H	H	H	CF_3	OMe	S	-0.94
28	H	H	NO_2	H	OMe	S	0.49

Figure 2 shows the histogram of frequencies of log (IC_{50}).

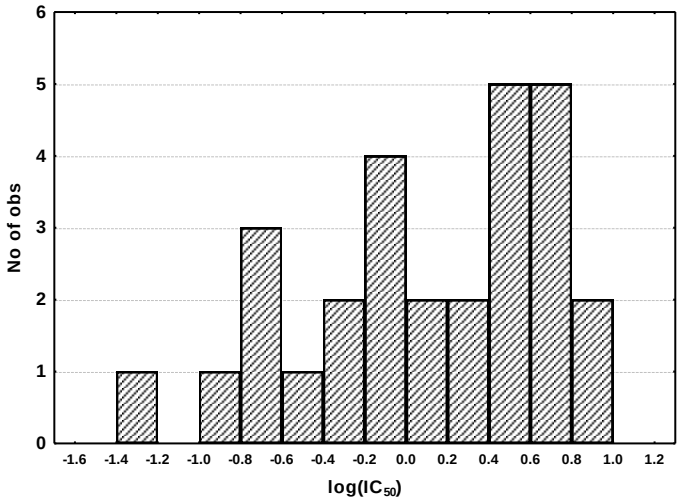

Figure 2: log(IC_{50}) data. Histogram of frequencies

Figure 3 shows the Box-Whiskers plot of log(IC_{50}) values with median and quartile values.

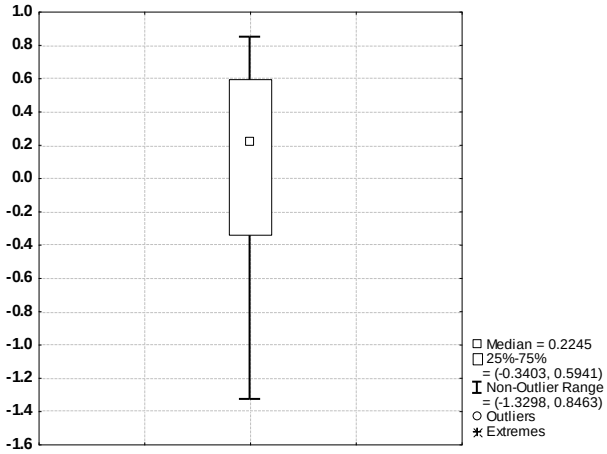

Figure 3: Log(IC_{50}) data. Box-Whiskers plot

These plots provide a better vision of the homogeneity of the data distribution.

The method [18].

The Klopman-Peradejordi-Gómez (KPG) QSAR method is based on the following linear equation [19-24]:

$$\log(IC_{50})=a+b\log\left(M_D\right)+\sum_{o=1}^{sub}\varphi_o+\sum_{i=1}^{Y}\left[e_iQ_i+f_iS_i^E+s_iS_i^N\right]+$$
$$+\sum_{i=1}^{Y}\sum_{m=(HOMO-2)^*,i}^{(HOMO)^*,i}\left[h_i\left(m\right)F_i(m^*)+j_i\left(m\right)S_i^E\left(m^*\right)\right]+$$
$$+\sum_{i=1}^{Y}\sum_{m'=(LUMO)^*,i}^{(LUMO+2)^*,i}\left[r_i\left(m'\right)F_i(m'^*)+t_i\left(m'\right)S_i^N\left(m'^*\right)\right]+$$
$$+\sum_{i=1}^{Y}\left[g_i\mu_i^*+k_i\eta_i^*+o_i\omega_i^*+z_i\zeta_i^*+w_jQ_i^{*,max}\right] \quad (1)$$

where $\log(IC_{50})$ is the biological activity, M_D is the drug's mass and φ_o is the orientational parameter of the o-th substituent (the summation runs over all the substituents selected for the research). Q_i is the net charge of atom I, S_i^E and S_i^N are, respectively, the total atomic electrophilic and nucleophilic superdelocalizabilities of atom i. F_{i,m^*} is the electron population of atom i in occupied (empty) local MO m* (m'*), $S_i^E(m)^*$ is the orbital electrophilic superdelocalizability at occupied local MO m* of atom i and $S_i^N(m')^*$ is the orbital nucleophilic superdelocalizability at empty local MO m'* of atom i. μ_i^*, η_i^*, ω_i^*, ζ_i^* and $Q_i^{*,max}$ are, respectively, the local atomic electronic chemical potential, the local atomic hardness, the local atomic electrophilicity, the local atomic softness and the maximal amount of electronic charge that atom i may accept. These indices were developed within the Hartree-Fock formalism [24]. Nevertheless, they can be calculated at the DFT level of theory [24]. The molecular orbitals with an asterisk are the Local Molecular Orbitals (LMO) of each atom. For atom x, the LMOs are defined as the subset of the molecule's MOs having an electron population greater than 0.01e on x. For example, let us consider the highest occupied molecular orbital (HOMO) of molecule 1 shown below.

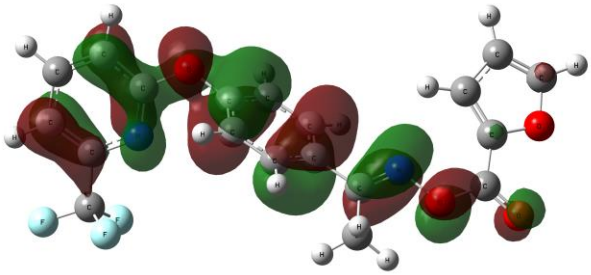

Figure 4: Highest occupied molecular orbital of molecule 1

For the purposes of the example, we are going to assume that the population analysis showed that the electronic population of each atom in which the MO is localized is greater than 0.01. Therefore, this molecular HOMO is at the same time the local (HOMO)* of these atoms. The local (HOMO)* of each one of the remaining atoms, which does not correspond to the molecular HOMO, will correspond to the highest occupied molecular MO having an electron population greater than 0.01 on them.

In this study we have considered the three highest occupied local MOs ((HOMO)*, (HOMO-1)*, (HOMO-2)*) and the three lowest empty local MOs ((LUMO)*, (LUMO+1)*, (LUMO+2)*) of each atom because experimental evidence indicates that they are determinant for molecular reactivity. The index Y in the summations runs over all atoms composing the molecule.

The KPG method has produced excellent results for a variety of molecules and biological activities [25-50].

Calculations [18].

The electronic structure of all molecules was calculated within the Density Functional Theory at the B3LYP/6-311g(d,p) level after full geometry optimization at the same level of theory. The Polarizable Continuum Model, using the integral equation formalism variant with water as solvent, was used in all calculations. The Gaussian suite of programs was used [51]. The numerical values of the local atomic reactivity indices were obtained from the Gaussian results with the D-Cent-QSAR software [52]. All the electron populations smaller than or equal to 0.01 e were considered as zero. Negative or greater than 2.0 electron populations coming from Mulliken Population Analysis were corrected as habitual [53]. Given that the resolution of the system of linear equations 1 is not possible, we made use of Linear Multiple Regression Analysis (LMRA) techniques to find the best solution. A matrix containing the dependent variable and the local atomic reactivity indices of all atoms of the common skeleton as independent variables was built. The Statistica software was used for LMRA [54].

We worked within the common skeleton concept: a definite collection of atoms common to all molecules analyzed accounting for about all the biological activity. Then, distinct parts or this common skeleton should account for almost all the interactions leading to the expression of a given biological activity [55]. The common skeleton for biphenyl ether derivatives is shown in Fig. 5.

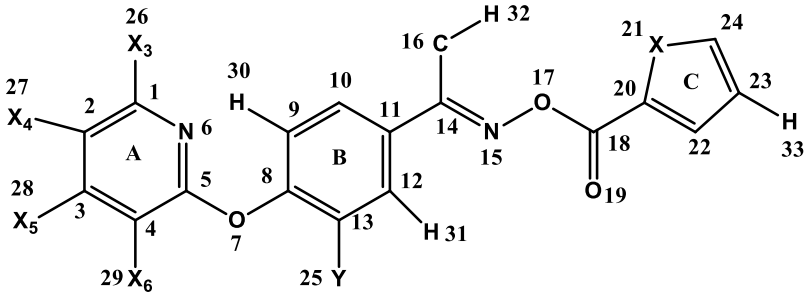

Figure 5: Common skeleton of biphenyl ether derivatives

The choice of the common skeleton is made by the researchers. It is suggested to include the largest number of atoms to detect different kinds of possible interactions. In the case of Y, X_3, X_4, X_5 and X_6 in Table 1, only the atom directly bonded to the skeleton is considered.

Results

The best equation obtained was:

$$\log(IC_{50}) = 0.91 - 0.03S_5^N - 1.67F_4(HOMO-2)^* - 0.007S_{26}^N(LUMO+2)^* - 0.02S_{28}^E + 0.01S_4^N(LUMO+1)^* - 0.32F_{29}(LUMO+2)^* \quad (2)$$

with n=19, R=0.99, R^2=0.99, adj-R^2=0.98, F(6,12)=178.22 (p<0.00000) and SD=0.05. No outliers were detected, and no residuals fall outside the ±2σ limits. Here, S_5^N is the total atomic nucleophilic superdelocalizability of atom 5, F_4(HOMO-2)* is the Fukui index (the electron population) of the third highest occupied local MO of atom 4, S_{26}^N(LUMO+2)* is the nucleophilic superdelocalizability of the third lowest empty local MO of atom 26, S_{28}^E is the total atomic electrophilic superdelocalizability of atom 28, S_4^N(LUMO+1)* is the nucleophilic superdelocalizability of the second lowest empty local MO of atom 4 and F_{29}(LUMO+2)* is the Fukui index (the electron population) of the third highest occupied local MO of atom 29.

Tables 2 and 3 show, respectively, the beta coefficients, the results of the t-test for significance of coefficients and the matrix of squared correlation coefficients for the variables of Eq. 2. There are no significant internal correlations between independent variables (Table 3). Figure 6 displays the plot of observed vs. calculated log(IC_{50}) values.

Table 2: Beta coefficients and t-test for significance of coefficients in Eq. 2

	Beta	**t(12)**	**p-level**
S_5^N	-0.76	-20.02	0.000000
F_4(HOMO-2)*	-0.51	-15.04	0.000000
S_{26}^N(LUMO+2)*	-0.39	-11.47	0.000000
S_{28}^E	-0.21	-6.07	0.00006
S_4^N(LUMO+1)*	0.18	4.90	0.0004
F_{29}(LUMO+2)*	-0.18	-4.66	0.0006

Table 3: Matrix of squared correlation coefficients for the variables in Eq. 2

	S_5^N	**F_4(HOMO-2)***	**S_{26}^N(LUMO+2)***	**S_{28}^E**	**F_{29}(LUMO+2)***
S_5^N	1				
F_4(HOMO-2)*	0.00	1.00			
S_{26}^N(LUMO+2)*	0.00	0.00	1.00		
S_{28}^E	0.00	0.00	0.01	1.00	
F_{29}(LUMO+2)*	0.03	0.00	0.01	0.00	1.00
S_4^N(LUMO+1)*	0.02	0.01	0.00	0.00	0.00

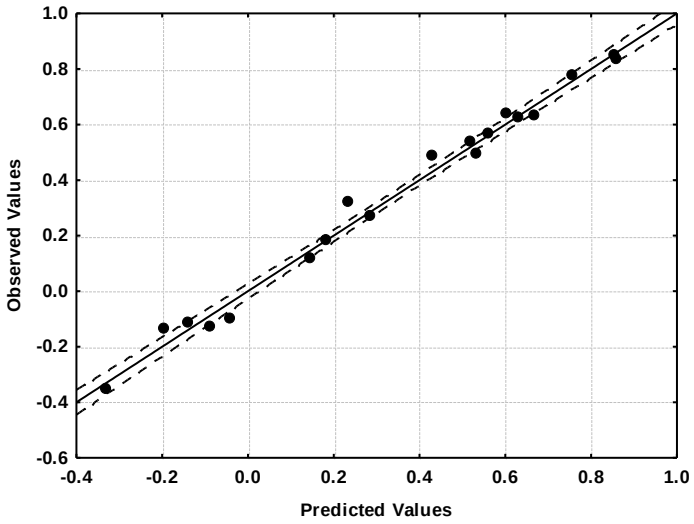

Figure 6: Plot of predicted vs. observed log(IC_{50}) values (Eq. 2). Dashed lines denote the 95% confidence interval.

The associated statistical parameters of Eq. 2 indicate that this equation is statistically significant and that the variation of the numerical values of a group of six local atomic reactivity indices of atoms constituting the common skeleton explains about 98% of the variation of log(IC_{50}). We need to provide evidence showing that the linear system of equations 1 gives superior results in this case. As we said in other papers, a "good regression analysis minimizes the residuals and it is expected that they be distributed as in a cloud showing no definite pattern or slope, centered (more or less) along of the horizontal axis (the x-axis is that of the values predicted by the regression equation) in a plot of predicted values vs. residuals scores. A random pattern indicates that the use of a linear model is correct. The plot of residuals versus deleted residuals shows the stability of the regression coefficients. No large discrepancies should appear between the residuals and the deleted residuals. Finally, we can use a normal probability plot of residuals to assess the normality of the distribution of a variable. If the observed residuals are distributed normally, they should fall on a straight line" [50]. Figures 7, 8 and 9 show, respectively, the plot of predicted values vs. residuals scores, the plot of residual vs. deleted residuals and the normal probability plot of residuals.

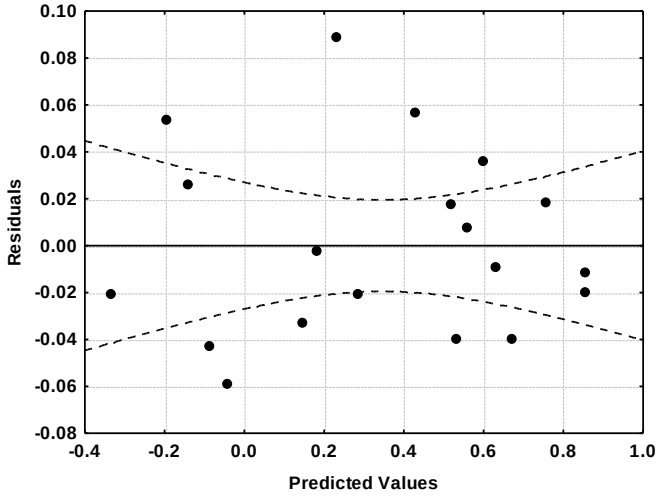

Figure 7: Plot of predicted values vs. residuals scores

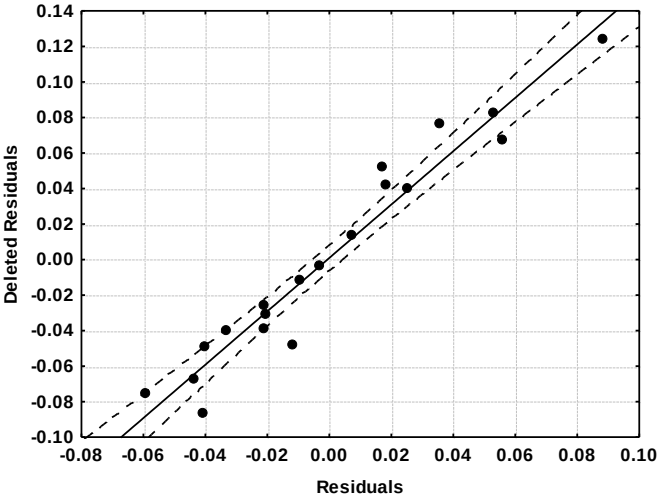

Figure 8: Plot of residuals vs. deleted residuals

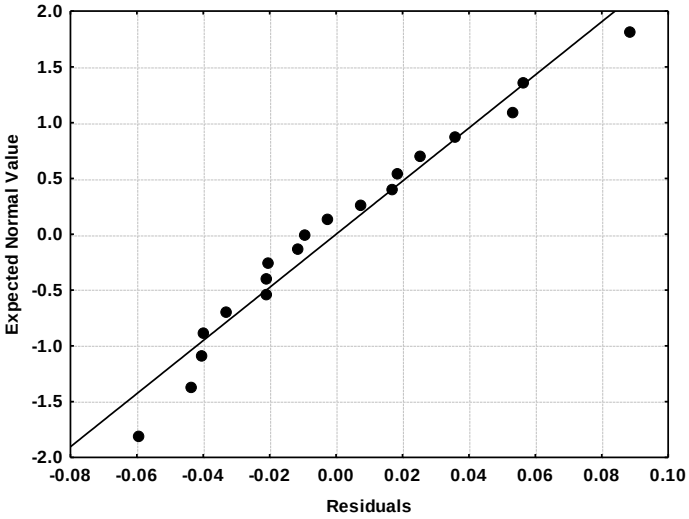

Figure 9: Normal probability plot of residuals

Figures 7 to 9 permit to state that the linear equation 2 is a good approximation to study this biological data and show that the regression coefficients are stable.

Local Molecular Orbitals. I.

We work with the hypothesis that any algebraic condition imposed on the numerical values of a reactivity index belonging to an inner occupied local MO or to an upper empty local MO of a given atom, also holds for the corresponding local MOs having a lower energy.

Tables 4 and 5 show the local MO structure of atoms 4, 5, 26, 28 and 29 (see Fig. 5). Nomenclature: Molecule (HOMO) / (HOMO-2)* (HOMO-1)* (HOMO)* - (LUMO)* (LUMO+1)* (LUMO+2)*. Lp (or lp) means lone pair.

Table 4: Local Molecular Orbitals of atoms 4, 5 and 26

Mol.	Atom 4 (C sp^2)	Atom 5 (C sp^2)	Atom 26
1 (100)	97π98π100π-102π103π104π	96σ98π100π-101π102π103π	94σ96σ98σ-102σ105σ114σ
2 (100)	96σ97π98π-102π103π104π	96σ97π98π-102π103π104π	82σ84σ96σ-108σ109σ110σ
3 (100)	97π98π100π-102π103π104π	96σ98π100π-101π102π104π	83σ84σ96σ-108σ109σ110σ
4 (100)	96σ97π98π-102π104π105π	97π98π100σ-102π104π105π	85σ86σ96σ-108σ109σ110σ
5 (95)	92π93π95π-96π99π100π	92π93π95π-97σ98π99π	87σ88σ89σ- 96π99π100π
6 (88)	86π87π88π-91π92π93π	86π87π88π-90π91π92π	83σ84σ86σ- 91σ115σ119σ
7 (88)	85σ86π88π-91π92π93π	85σ86π88π-90π91π92π	76σ77σ84σ- 96σ97σ99σ
8 (101)	97σ99π101π-103π104π105π	97σ99π101π-102σ103π104π	98π99π101π-104π106σ107σ
9 (92)	89π90π92π-94π95π96π	88π90π92π-93π94π95π	73σ74σ87σ- 98σ103σ104σ
10 (104)	101π102π104π-106π107π108π	99σ102π104π-106π107σ108π	96σ98σ99σ-106σ107σ109σ
11 (104)	100π102π104π-107π108π109π	100π102π104σ-106σ107π108π	82σ87σ99σ-113σ114σ115σ
12 (104)	100π102π104π-106π107π108π	99σ102π104π-106π107σ108π	85σ87σ99σ-113σ114σ115σ
13 (104)	99σ100π102π-107π108π109π	100π102π104σ-106σ107π108π	88σ91σ99σ-113σ114σ115σ
14 (92)	90π91π92π-95π97π111π	88σ91π92π-94π95π96π	86σ87σ91σ- 95σ120σ121σ
15 (92)	88σ90π92σ-95π96π97π	88σ90π92σ-94σ95π96π	79σ80σ87σ-101σ102σ104σ
16 (105)	103π104π105π-108π109π110π	103π104π105π-107σ108π109π	103π104π105π-108π110σ111σ
17 (96)	92π94π96π-99π100π101π	91π94π96π-98π99π100π	75σ76σ90σ-102σ108σ109σ
18 (108)	105π106π108π-110π112π126σ	105π106π108σ-110π111σ112π	102σ104σ105π-110π112π124σ
19 (108)	104σ105π106π-111π112π113π	105π106π108σ-109σ110σ111π	91σ93σ104σ-116σ118σ119σ
20 (108)	105π106π108π-110π111π112π	105π106π108σ-109σ110π112π	91σ93σ104σ-116σ118σ120σ
21 (108)	104σ105π106π-	105π106π108σ-	93σ94σ104σ-116σ118σ119σ

	110π111π112π	110π111σ112π	
22 (103)	96σ100π101π- 104π107π108π	100π101π103σ- 105σ106π107π	93σ96σ97σ-104π107π108π
23 (103)	99σ100π101π- 104π107π108π	100π101π103σ- 104π106σ107π	96σ97σ99σ-112σ114σ115σ
24 (112)	109π111π112π- 115π116π132π	109π111π112σ- 114σ115π116π	106σ107σ109σ- 115σ116σ130σ
25 (112)	107σ109π111π- 115π116π128σ	109π111π112σ- 114σ115π116π	96σ97σ107σ-121σ123σ124σ
26 (112)	109π111π112π- 114π115π116π	109π111π112σ- 114π115σ116σ	96σ97σ107σ-121σ123σ124σ
27 (112)	107σ109π111π- 114π115π116π	109π111π112σ- 114σ115π116π	96σ97σ107σ-121σ123σ124σ
28 (107)	103π104π106π- 108π111π112π	104π106π107σ- 108π110σ111π	83σ101σ102σ- 117σ119σ120σ

Table 5: Local Molecular Orbitals of atoms 28 and 29

Mol.	**Atom 28**	**Atom 29**
1 (100)	84σ85σ87σ- 108σ109σ110σ	85σ92σ96σ- 108σ109σ110σ
2 (100)	81σ82σ96σ- 108σ109σ110σ	77σ84σ96σ- 108σ109σ110σ
3 (100)	83σ84σ91σ- 102σ104σ114σ	83σ84σ96σ- 108σ109σ110σ
4 (100)	82σ83σ96σ- 108σ109σ110σ	85σ86σ96σ- 102σ104σ105σ
5 (95)	76σ85σ86σ- 104σ105σ106σ	75σ83σ85σ- 104σ105σ106σ
6 (88)	74σ75σ84σ- 96σ97σ98σ	73σ75σ84σ- 96σ97σ98σ
7 (88)	78σ83σ84σ- 111σ112σ113σ	76σ77σ84σ- 96σ97σ100σ
8 (101)	82σ83σ91σ- 107σ110σ111σ	83σ91σ97σ- 110σ111σ112σ
9 (92)	82π87σ88π- 95π96lp98σ	71σ73σ87σ- 98σ103σ104σ
10 (104)	82σ85σ87σ- 113σ114σ115σ	87σ96σ99σ- 113σ114σ115σ
11 (104)	85σ87σ99σ- 113σ114σ115σ	80σ87σ99σ- 113σ114σ115σ
12 (104)	84σ87σ95- 106σ107σ108σ	85σ87σ99σ- 113σ114σ115σ
13 (104)	82σ85σ 99σ- 113σ114σ115σ	87σ88σ99σ- 107σ108σ109σ
14 (92)	77σ78σ87σ- 101σ102σ103σ	76σ78σ87σ- 101σ102σ104σ
15 (92)	82σ86σ87σ- 115σ117σ118σ	72σ79σ87σ- 101σ102σ105σ
16 (105)	84σ86σ95σ- 111σ115σ116σ	86σ95σ100σ- 115σ116σ117σ
17 (96)	86π90σ91π- 99π100lp102σ	75σ76σ90σ- 102σ109σ111σ
18 (108)	88σ89σ92σ- 116σ117σ118σ	93σ101σ102σ- 117σ118σ119σ
19 (108)	89σ91σ104σ-	90σ91σ104σ-

	116σ118σ119σ	118σ119σ120σ
20 (108)	91σ92σ99π-	88σ89σ104σ-
	110σ112σ122σ	118σ119σ121σ
21 (108)	88σ89σ104σ-	93σ94σ104σ-
	116σ118σ120σ	110σ112σ122σ
22 (103)	81σ82σ93σ-	79σ81σ93σ-
	112σ113σ114σ	112σ113σ114σ
23 (103)	91π92σ94σ-	78σ81σ99σ-
	104π107π108π	114σ117σ118σ
24 (112)	88σ91σ95σ-	93σ95σ106σ-
	121σ122σ123σ	122σ123σ124σ
25 (112)	91σ94σ107σ-	93σ94σ107σ-
	121σ123σ124σ	123σ124σ125σ
26 (112)	94σ95σ103π-	91σ93σ107σ-
	114σ115π116σ	123σ124σ125
27 (112)	90σ91σ107σ-	96σ97σ107σ-
	121σ123σ124σ	115σ116σ128σ
28 (107)	95π96σ98σ-	83σ101σ102σ-
	108π111π112π	119σ120σ121σ

Molecules that did not participate in the generation of Eq. 2

Figure 10 shows the histogram of frequencies of the excluded log(IC_{50}) data (data excluded during the generation of Eq. 2). These molecules are 4, 7, 13, 17, 19, 21 and 25-27 of Table 1 (n=9).

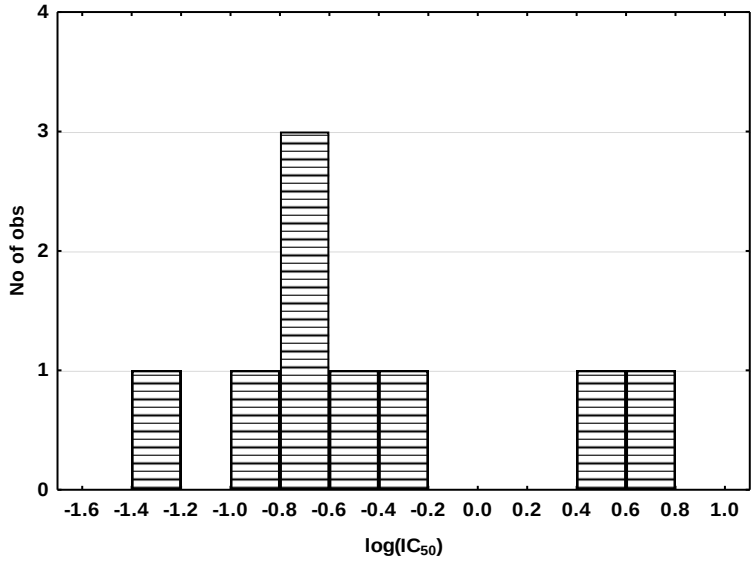

Figure 10: Log(IC50) data. Histogram of frequencies of the excluded data

We can see that the log(IC_{50}) values not used to generate equation 2 are distributed along the same interval as the values considered for that purpose. This is important because if, for example, the values not considered were within a small interval that is on the extreme right or left of the distribution of the experimental data, the possibility of the existence of a second mechanism of action would have to be considered.

Conformational aspects

The optimized geometries employed here were obtained for calculations conducted with water as solvent. The conformation of each molecule at the active site is not known. However, equation 2 strongly suggests that the molecules with which Equation 2 was generated are all similarly aligned. Therefore, it is interesting to compare the

optimized geometries. Figure 1 shows the approximate superimposition of atoms 1 to 3 of molecules 2-9 to molecule 1 (see Fig. 5). Molecule 1 is an arbitrary choice [56].

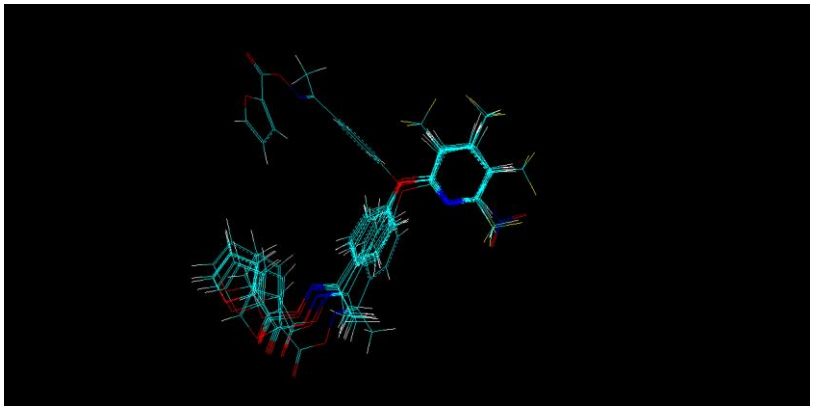

Figure 11: Approximate superimposition of atoms 1, 2 and 3 of molecules 2-9 on molecule 1.

Molecule 2 (see Table 1) is pointing toward a different direction. Figure 12 shows the approximate superimposition of atoms 1 to 3 of molecules 10-17 on molecule 1 (see Fig. 5).

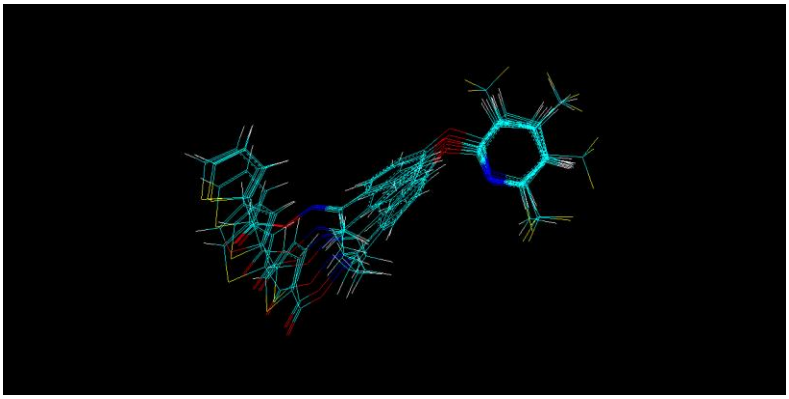

Figure 12: Approximate superimposition of atoms 1, 2 and 3 of molecules 10-17 on molecule 1

We can see that all molecules superimpose well. Figure 13 shows the approximate superimposition of atoms 1 to 3 of molecules 18-23 on molecule 1.

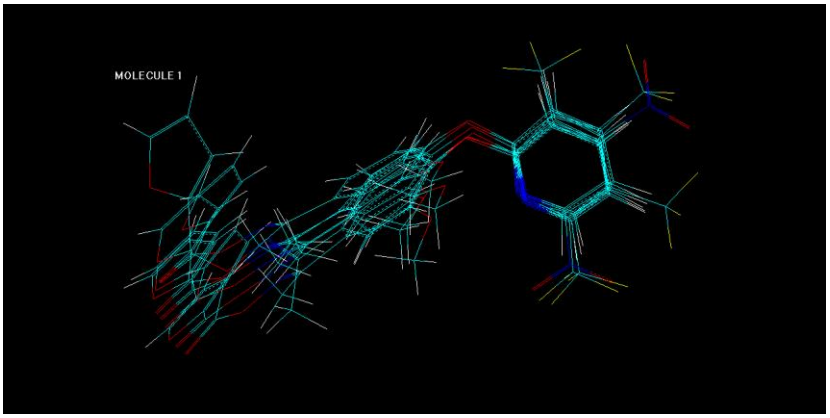

Figure 13: Approximate superimposition of atoms 1 to 3 of molecules 18-23 on molecule 1

Here, ring C of molecules 18-23 points toward a different point than ring C of molecule 1 as shown in the next figures.

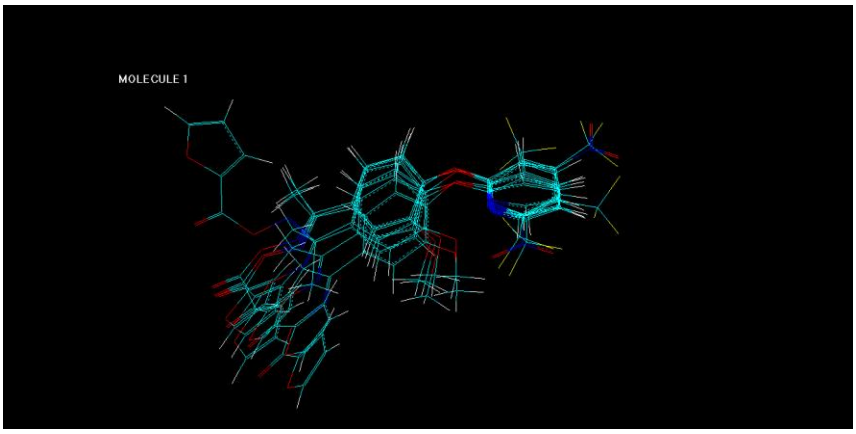

Figure 14: Approximate superimposition of atoms 1 to 3 of molecules 18-23 on molecule 1

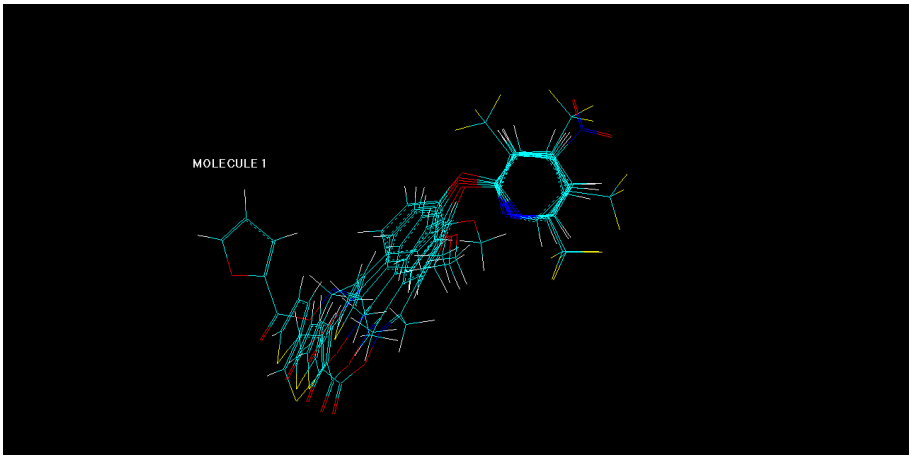

Figure 15: Approximate superimposition of atoms 1 to 3 of molecules 24-28 on molecule 1

We can see that, in general, it is not possible to make significant suggestions about relationships between conformation and activity. We need to explore other molecular properties such as the conformers.

From Table 1 we observe that molecule 14 is the less active one and that molecule 21 is the most active one regarding PPO inhibition. To compare their conformational behavior, we used MarvinView software v23.1 (with Dreiding Force Field, 'very strict' optimization limit and a diversity limit of 0.1, [57]) to get the first ten conformers of these molecules. In figures 16 to 18 we present the geometry of the optimized molecule 14 and its ten conformers [58].

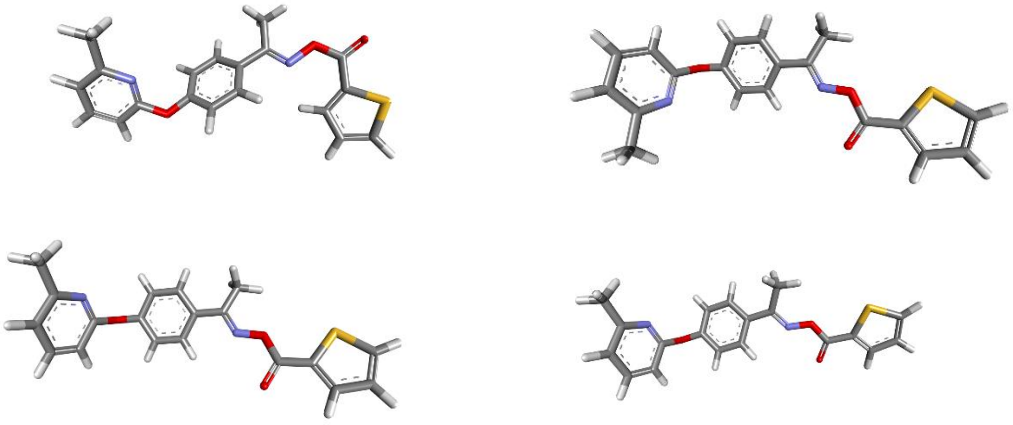

Figure 16: Molecule 14. Optimized geometry (upper left) and its first three conformers

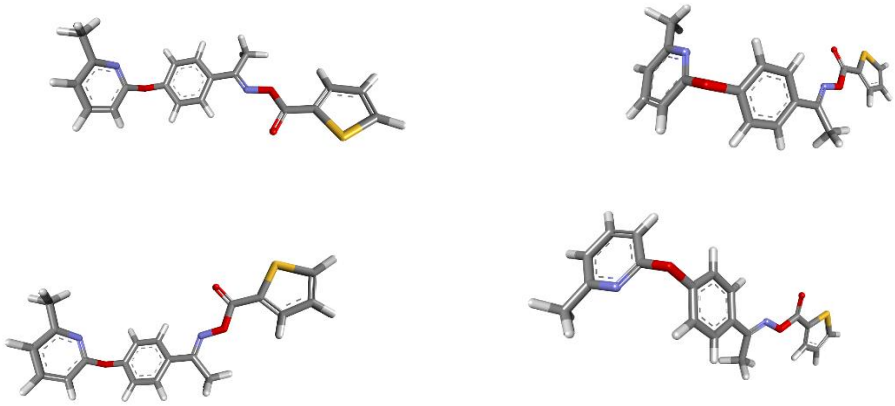

Figure 17: Molecule 14. Conformers 4 to 7

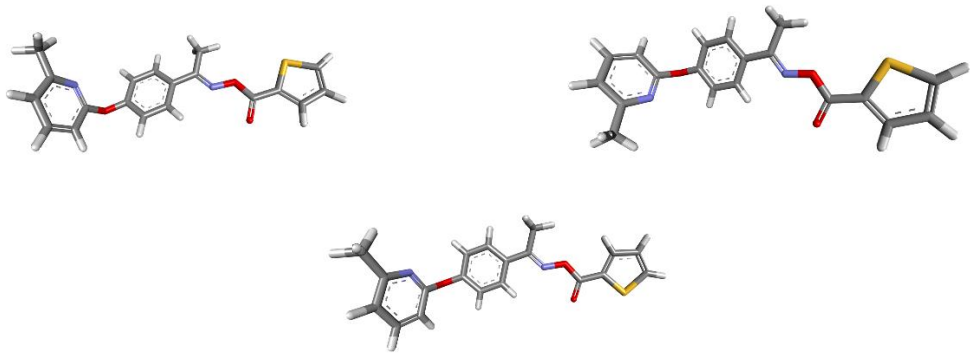

Figure 18: Molecule 14. Conformers 8 to 10.

We can see that, in general terms, the geometry-optimized molecule and its conformers have extended conformations. No intramolecular interaction is observed. In figures 19 to 21 we present the geometry of the optimized molecule 21 and its ten conformers.

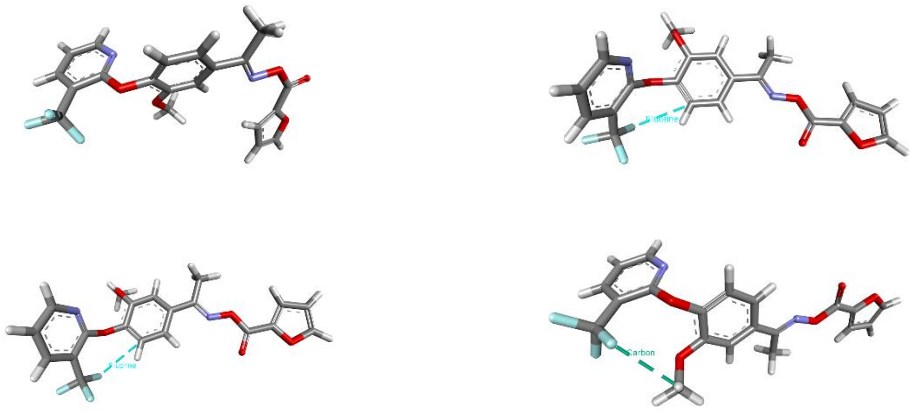

Figure 19: Molecule 21. Optimized geometry (upper left) and its first three conformers

In this figure, we can see that the optimized geometry has an approximately extended conformation. No intramolecular interactions are observed. In the case of the first two conformers, we see that an interaction C-F...C (3.47 and 3.48 Å) appears, which limits the conformational freedom of ring A. The third conformer has an interaction C-F...H2,82) which occurs at a smaller distance between the participants than in the case of conformers 1

and 2. This interaction also limits the rotational freedom of ring A. These two interactions appear in the conformers 4 to 10 (Fig. 20 and 21 below).

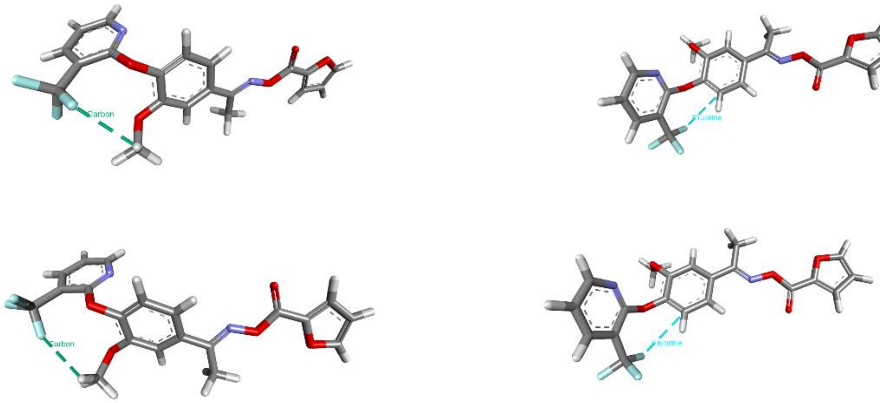

Figure 20: Molecule 21. Conformers 4 to 7.

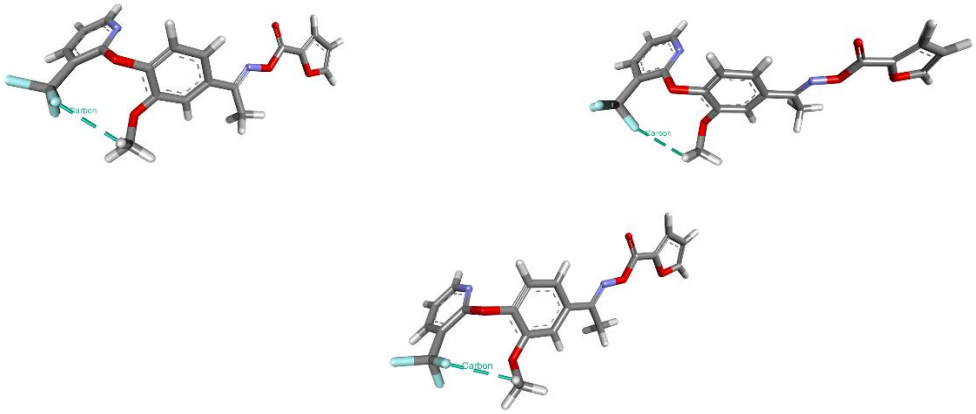

Figure 21: Molecule 21. Conformers 8 to 10.

An important conclusion would be that the conformers of the more active molecule have an intermolecular interaction that produces a certain relative position of the A and B rings. In the case of the less active molecule, only conformers with extended conformations appear. Noting in Table 1 that the -CF_3 substituent bonded in the R_3 position in molecule 1 has not a high inhibitory activity, we investigated its conformers. Figures 22 to 24 show the results of conformers search.

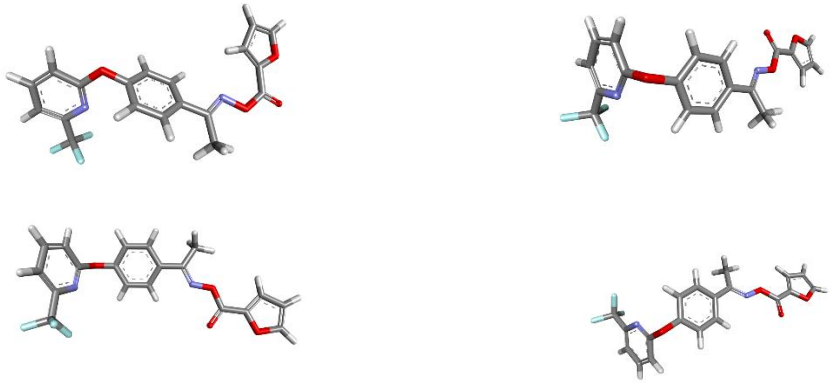

Figure 22: Molecule 1. Optimized geometry (upper left) and its first three conformers.

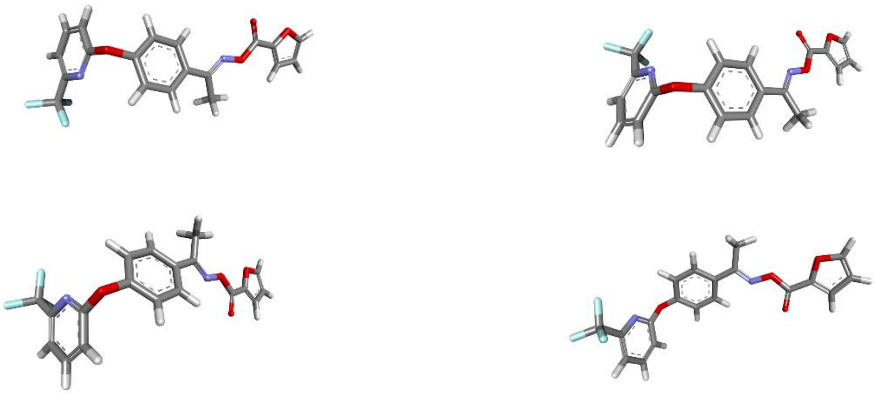

Figure 23: Molecule 1. Conformers 4 to 7

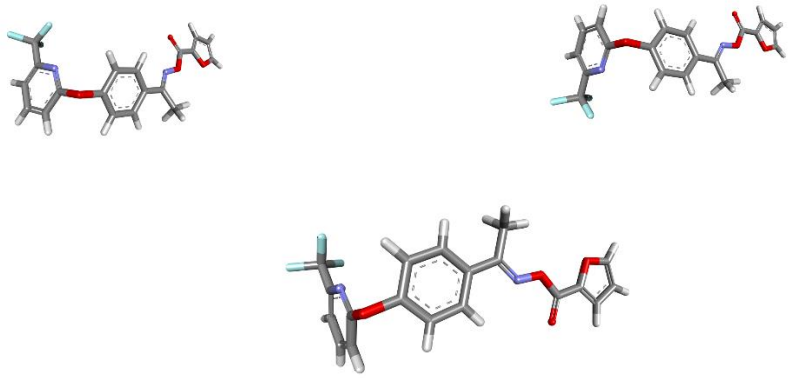

Figure 24: Molecule 1. Conformers 8 to 10

We can see that there are no conformers having intramolecular interactions because ring B has not a suitable substituent. In the case of molecule 18, we observed that it has a high inhibitory activity. Since it has a CF_3 group in position R_3, its first ten conformers were obtained to see if ring A could rotate to form some intramolecular bond with the OMe group of ring B. Figures 25 to 27 show the results.

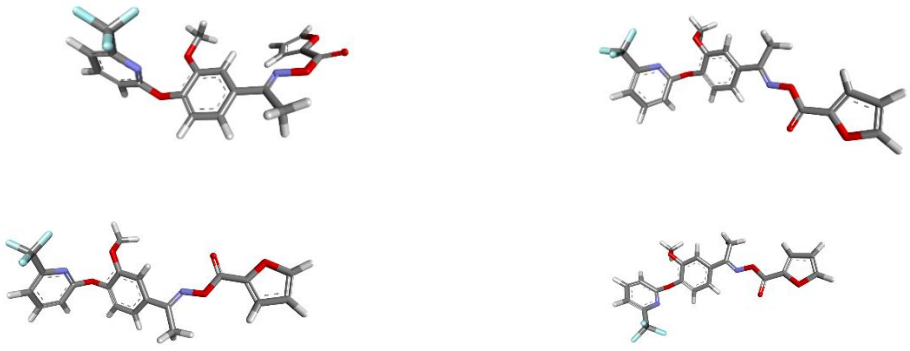

Figure 25: Molecule 18. Optimized geometry (upper left) and its first three conformers.

Figure 26: Molecule 18. Conformers 4 to 7

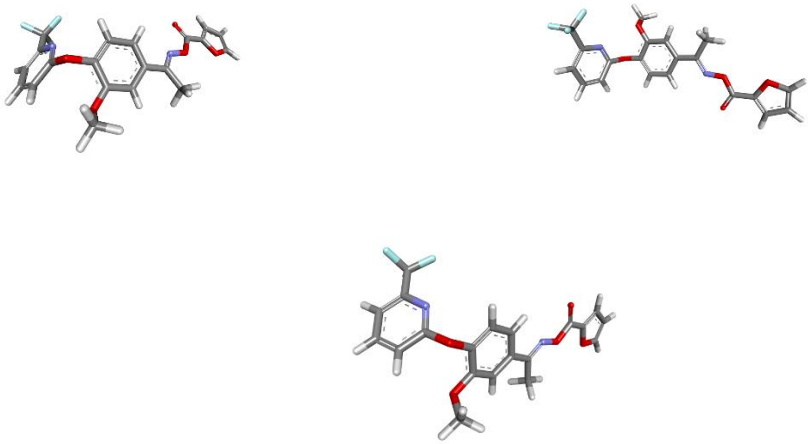

Figure 27: Molecule 18. Conformers 8 to 10.

No intramolecular interactions are observed in any structure, because the distance between the potential participants is too great.

A correct suggestion for experimentalists is to find a way to keep the relative orientation of rings A and B fixed. For example, a substituent of the form Ring A-CF_2-CH_2-CH_2-O-Ring B seems appropriate.

Frontier Molecular Orbitals

Table 6 shows the main localization of HOMO and LUMO on rings A-C (see Fig. 5 for ring numbering). Capital letters indicate a localization with high electron density. Lowercase letters indicate low electron density. This is a qualitative appreciation.

Table 6: Main localization of the Frontier Molecular Orbitals.

Mol	HOMO	LUMO	log(IC_{50})
1	A, B	B, C	0.27
2	B, C	B, C	-0.14
3	A, B, c	B, C, a	0.11
4	B, C, a	B, C	-0.51
5	A, B, c	A	0.62
6	A, B	B, C	0.78
7	A, B	B, C	0.76
8	A, B	B, C	0.63
9	A, B	B, C	0.54

10	A, B	B, C	0.32
11	a, B, c	B, C	-0.10
12	A, B	B, C	0.18
13	a, B	B, C	-0.67
14	A, B	B, C	0.85
15	A, B	B, C	0.84
16	A, B	B, C	0.64
17	A, B	B, C	0.54
18	a, B	B, C	-0.13
19	B	B, C	-0.74
20	a, B	B, C	-0.35
21	a, B	B, C	-1.33
22	a, B	A	0.57
23	a, B	A	0.49
24	a, B	B, C	-0.11
25	a, B	B, C	-0.66
26	a, B	B, C	-0.33
27	a, B	B, C	-0.94
28	a, B	A	0.49

The first point to state is that *all* molecules have PPO inhibitory activity. We may note that the molecular LUMO is localized on rings B and C in almost all molecules. In four of them, it is localized only on ring A. This could mean that, if rings B and/or C are interacting with the site through an empty MO, this MO will correspond to a higher empty one. The molecular HOMO is localized on rings A and B with the only exception of molecule 19. These are examples showing the possible chemical role of MOs other than the frontier ones.

To get more information about the inhibitory mechanism, and using Table 6, we conducted the following two new LMRAs. In the first one, we used a set of molecules with only negative values for $\log(IC_{50})$. In the second one, molecules with only positive values for $\log(IC_{50})$ without including the molecules with LUMO localized only on ring A were analyzed.

LMRA for molecules with only negative values for $\log(IC_{50})$.

Molecules 2, 4, 11, 13 18-21 and 24-27 were employed. The best equation obtained is:

$$\log(IC_{50}) = 1.66 - 1.54F_{28}(LUMO+1)^* - 0.05S_6^N(LUMO+1)^* - 2.46Q_2^{max} \quad (3)$$

with n=12, R=0.98, R^2=0.97, adj-R^2=0.96, F(3,8)=85.186 (p<0.00000) and SD=0.08. No outliers were detected, and no residuals fall outside the ±2σ limits. Here, Q_2^{max} is the maximal amount of electronic charge that atom 2 may accept, $F_{28}(LUMO+1)^*$ is the Fukui index of the second lowest empty local MO localized on atom 28 and $S_6^N(LUMO+1)^*$ is the nucleophilic superdelocalizability of the second lowest empty local MO localized on atom 6. Tables 7 and 8 show the beta coefficients, the results of the t-test for significance of coefficients and the matrix of squared correlation coefficients for the variables of Eq. 3. There are no significant internal correlations between independent variables. Figure 28 displays the plot of observed *vs.* calculated $\log(IC_{50})$.

Table 7: Beta coefficients and t-test for significance of coefficients in Eq. 3

Variable	Beta	t(8)	p-value
$F_{28}(LUMO+1)^*$	-1.06	-15.84	0.000000
$S_6^N(LUMO+1)^*$	-0.31	-4.68	0.002

Table 8: Matrix of squared correlation coefficients for the variables in Eq. 3

	Q_2^{max}	$S_6^N(LUMO+1)^*$	$F_{28}(LUMO+1)^*$
Q_2^{max}	1.00		
$S_6^N(LUMO+1)^*$	0.01	1.00	
$F_{28}(LUMO+1)^*$	0.00	0.15	1.00

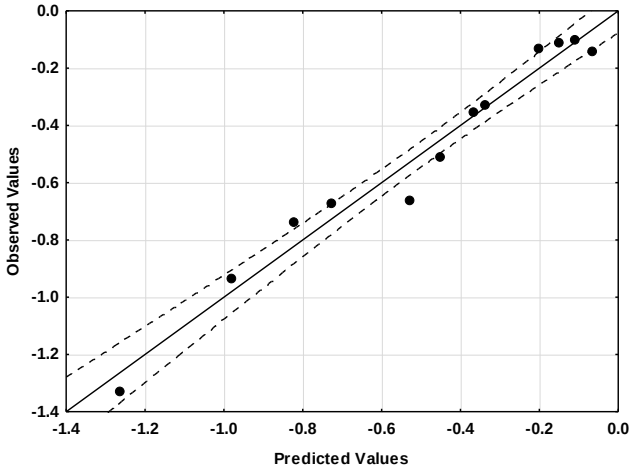

Figure 28: Plot of predicted vs. observed log(IC_{50}) values (Eq. 3). Dashed lines denote the 95% confidence interval.

The associated statistical parameters of Eq. 3 indicate that this equation is statistically significant and that the variation of the numerical values of a group of three local atomic reactivity indices of atoms constituting the common skeleton explains about 96% of the variation of log(IC_{50}). Figures 29, 30 and 31 show, respectively, the plot of predicted values vs. residuals scores, the plot of residual vs. deleted residuals and the normal probability plot of residuals.

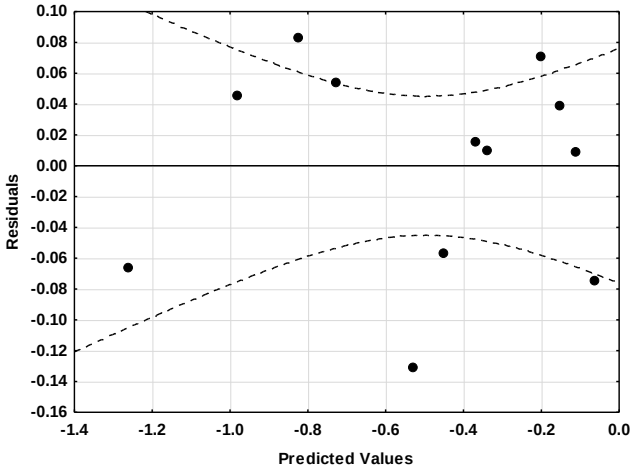

Figure 29: Plot of predicted values vs. residuals scores

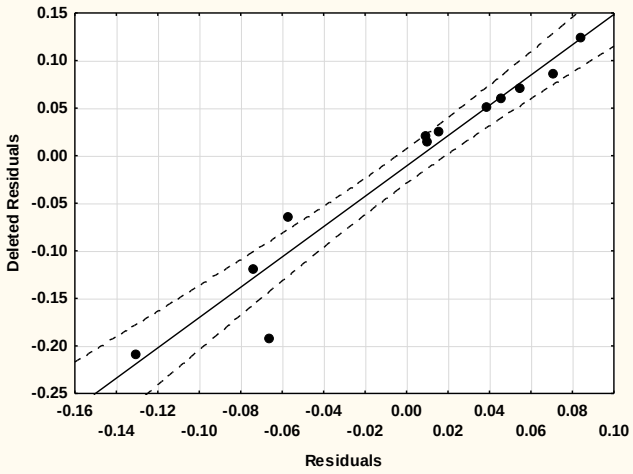

Figure 30. Plot of residuals vs. deleted residuals

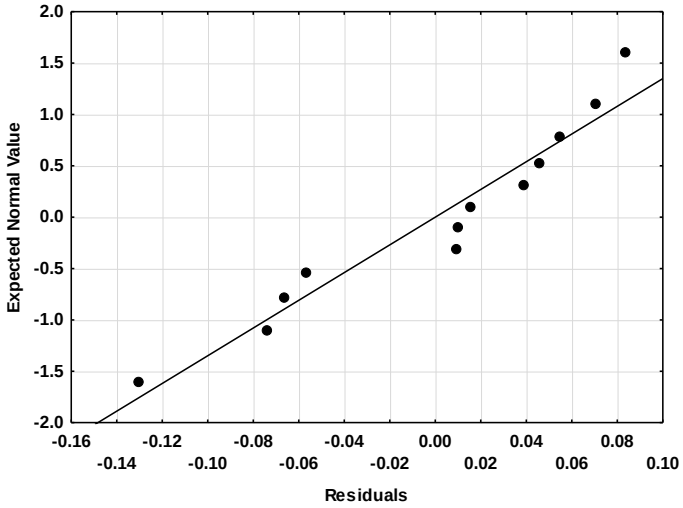

Figure 31. Normal probability plot of residuals

The above figures allow declaring that the linear equation 3 is a good approximation to study this biological data and show that the regression coefficients are stable.

LMRA for molecules with only positive values for log(IC_{50}) without including the molecules with LUMO localized only on ring A.

Molecules 1, 3, 6-10, 12, 14-17 were employed. The best equation obtained is:

$$\log(IC_{50}) = 1.18 + 4.23 S_{14}^{E}(HOMO)^* \quad (4)$$

with n=12, R=0.97, R^2=0.94, adj-R^2=0.93, F(1,10)=155.94 (p<0.00000) and SD=0.06. No outliers were detected, and no residuals fall outside the ±2σ limits. S_{14}^{E}(HOMO)* corresponds to the highest occupied local MO localized on atom 14. Table 9 shows the beta coefficient and the result of the t-test for significance of coefficient. Figure 32 displays the plot of observed *vs.* calculated log(IC_{50}).

Table 9: Beta coefficient and t-test for significance of coefficient in Eq. 4

	Beta	**t(10)**	**p-value**
S_{14}^{E}(HOMO)*	0.97	12.49	0.000000

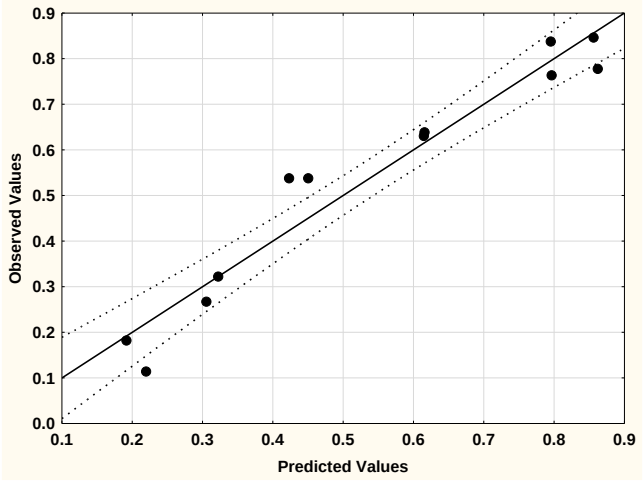

Figure 32: Plot of predicted vs. observed log(IC_{50}) values (Eq. 4). Dashed lines denote the 95% confidence interval

The associated statistical parameter of Eq. 4 indicates that this equation is statistically significant and that the variation of the numerical values of one local atomic reactivity index of atoms constituting the common skeleton explains about 93% of the variation of log(IC_{50}). Figures 33, 34 and 35 show, respectively, the plot of predicted values vs. residuals scores, the plot of residual vs. deleted residuals and the normal probability plot of residuals.

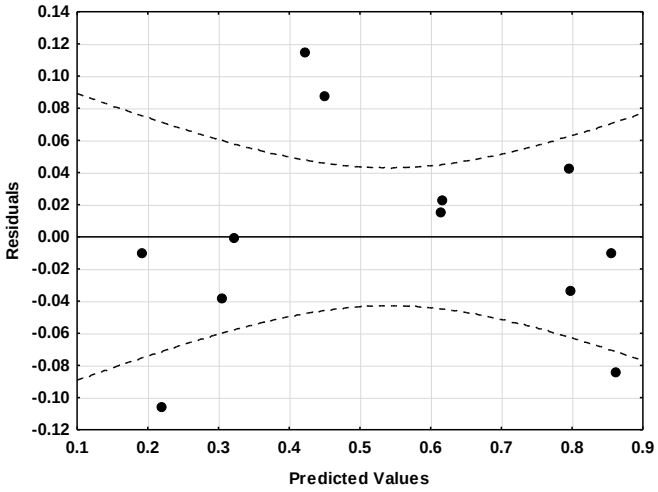

Figure 33: Plot of predicted values vs. residuals scores

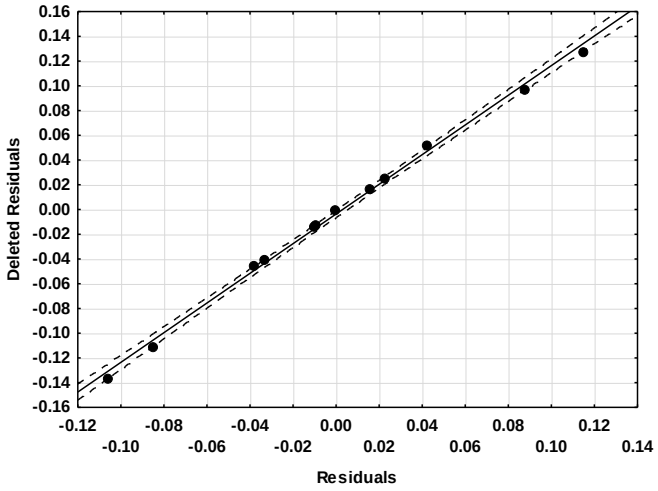

Figure 34: Plot of residuals vs. deleted residuals

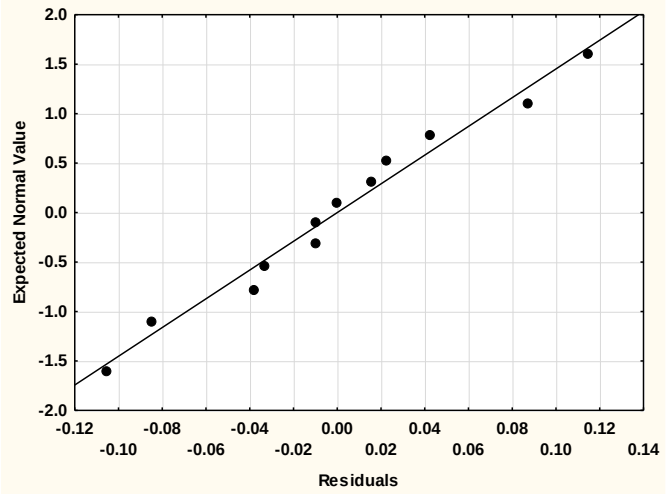

Figure 35. Normal probability plot of residuals

The above figures allow to declare that the linear equation 4 is a useful approximation to study this biological data and show that the regression coefficients are stable.

Local Molecular Orbitals. II.

Table 10 shows the local molecular orbitals of atoms participating in Eq. 3 and 4 (atom 28 is in another Table).

Table 10: Local Molecular Orbitals of atoms 2, 6 and 14.

Mol.	Atom 2 (C sp^2)	Atom 6 (N sp^2)	Atom 14 (C sp^2)
1 (100)	97π98π100π- 102π103π104π	97lp98π100π- 101π102σ104π	96σ98π100π- 101π103σ104σ
2 (100)	96σ97π98π- 102π103π104π	96σ97π98π- 102π103π104π	96π99π100π- 101π102π103π
3 (100)	97π98π100π- 102π104π105π	97lp98π100π- 101π102π103π	96π98π100π- 101π103σ106σ
4 (100)	97π98π100π- 102π104π105π	96σ98π100lp- 102σ104π105π	95π 96π100π- 101π103π106σ
5 (95)	92π93π95π- 96π98π99π	92π93π95π- 96π98π99π	91π93π95π- 97π98π99π
6 (88)	86π87π88π- 90π91π92π	85lp86lp88π- 90π91π92π	84σ86π88π- 89π90π91π
7 (88)	85σ86π88π- 90π91π92π	85lp86π88π- 90π91π92π	84π86π88π- 89π90π91π
8 (101)	97σ99π101π- 104π105π106π	98π99lp101π- 103π104π105π	97π99π101π- 102π103π104π
9 (92)	88π90π92π- 94π95π96π	89lp90π92π- 94π95π96π	87π90π92π- 93π94π95π
10 (104)	101π102π104π- 106π107π108π	100lp102π104π- 106π107π108π	99π102π104π- 105π106π107π
11 (104)	100π102π104σ- 107π108π109π	100lp102π104lp- 107π108π109π	98σ99π104π- 105π106π110σ
12 (104)	100π102π104π- 106π108π109π	100lp102π104π- 106π107π108π	99π102π104π- 105π106π107π
13 (104)	99σ100π102π- 107π108π109π	99lp102π104lp- 107π108π109π	98σ99π104π- 105π106π110σ
14 (92)	90π91π92π- 94π95π96π	88lp91lp92π- 94π95π96π	87π91π92π- 93π94π95π
15 (92)	88σ90π92π- 94π95π96π	88lp90π92π- 94π95π96π	87π90π92π- 93π94π95π
16 (105)	103π104π105π- 107π108π109π	100lp101lp105π- 107π108π109π	103π104π105π- 106π107π108π
17 (96)	91π94π96π- 98π99π100π	92lp94π96π- 98π99π100π	90π94π96π- 97π98π99π
18 (108)	105π106π108π- 110π112π113π	105π106π108lp- 110π112π124σ	105π106π108π- 109π111π112π
19 (108)	105π106π108π- 110π111π112π	105π106π108lp- 110π111π112π	105π106π108π- 109π110π112π
20 (108)	105π106π108π- 110π112π113π	105π106π108lp- 110π112π124σ	105π106π108π- 109π111π112π
21 (108)	105π106π108π- 110π112π113π	105π106π108lp- 110π111π112π	105π106π108π- 109π111π112π
22 (103)	97σ100π101π- 104π106π107π	100π101π103lp- 104π106π107π	100π101π103π- 105π106π107π
23 (103)	100π101π103π- 104π107π108π	100π101π103π- 104π107π108π	100π101π103π- 105π106π108π
24 (112)	109π111π112π-	109π111π112π-	109π111π112π-

	115π116π117π	114π115π116π	113π114π115π
25 (112)	109π111π112π-	109π111π112lp-	109π111π112π-
	114π115π116π	114π115π116π	113π114π116π
26 (112)	110π111π112π-	109π111π112π-	109π111π112π-
	114π115π116π	114π115π116π	113π114π115π
27 (112)	110π111π112π-	109π111π112lp-	109π111π112π-
	115π116π117π	115π116π132π	113π114π116π
28 (107)	104π106π107π-	104π106π107lp-	104π106π107π-
	108π111π112π	108π111π112π	109π110π112π

Molecular Electrostatic Potential (MEP)

The molecular electrostatic potential (MEP) gives a very general idea of the interactions in which a molecule can participate. The following figures show the MEP of the optimized geometries of the most active (molecule 21) and the least active molecule (molecule 14) in the plane defined by atoms 1, 2 and 3 [59]. They give an idea of the possible situation before reaching the receptor (inside the liquid biological milieu).

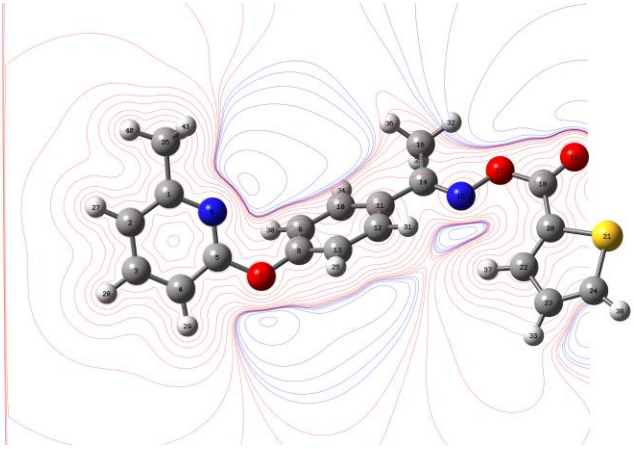

Figure 36: MEP of molecule 14 in the plane defined by atoms 1, 2 and 3 (isovalue = 0.02, red is a positive MEP value, blue is a negative MEP value)

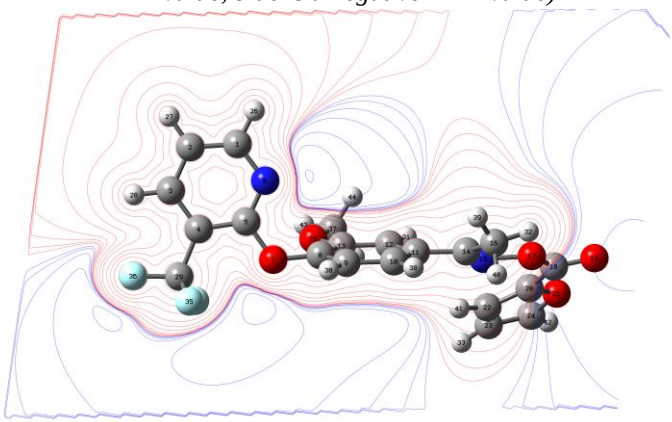

Figure 37: MEP of molecule 21 in the plane defined by atoms 1, 2 and 3 (isovalue = 0.02, red is a positive MEP value, blue is a negative MEP value)

Figures 38 to 41 show the MEP of molecules 14 and 21 at different distances from the nuclei [60].

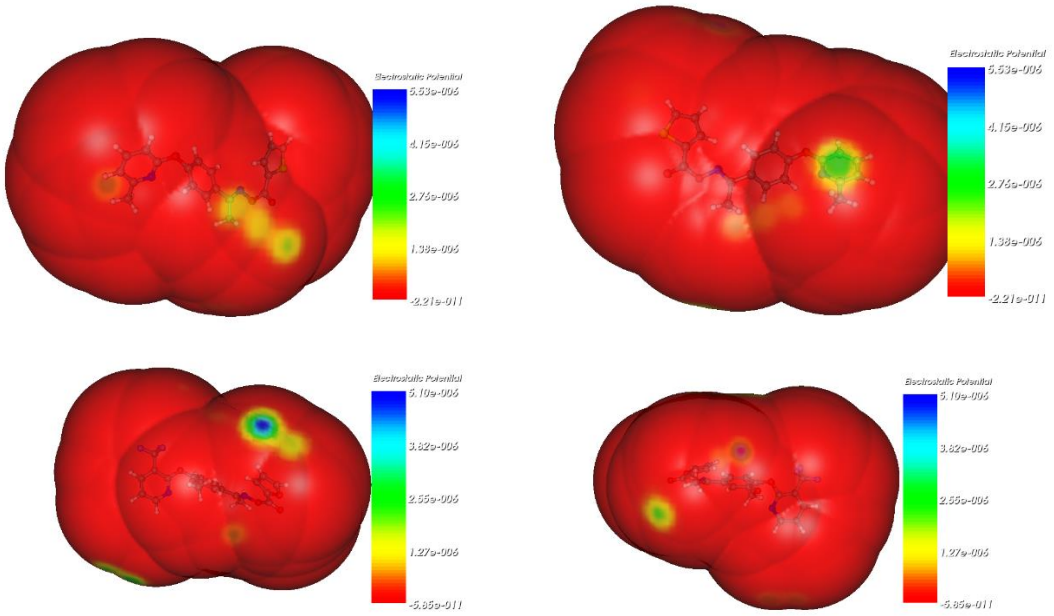

Figure 38: MEP map of molecules 14 (upper left: face side; upper right: back side) and 21 (lower left face side; lower right back side) at 5.5 Å of the nuclei.

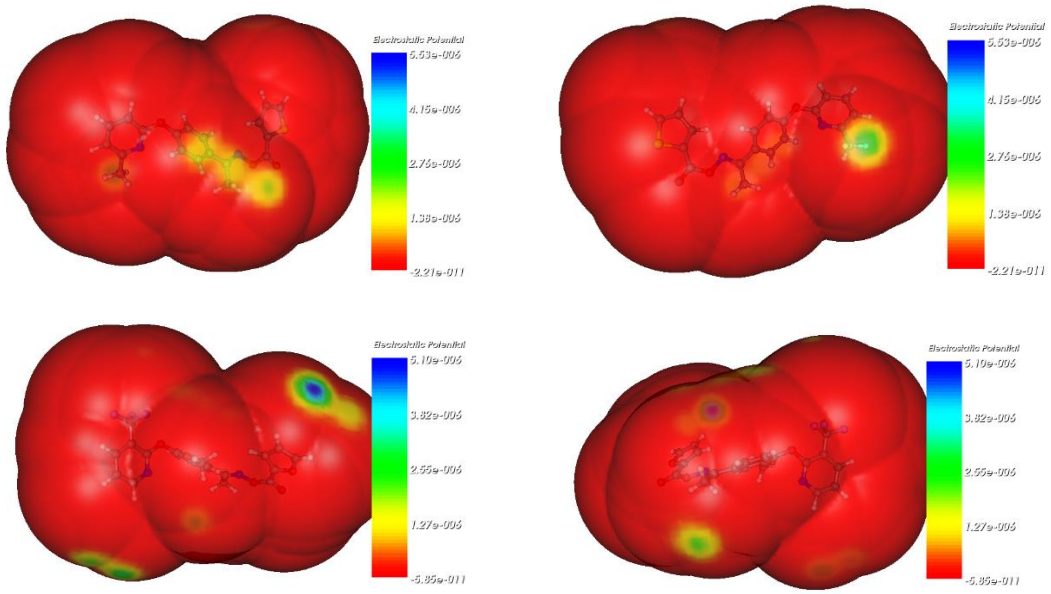

Figure 39: MEP map of molecules 14 (upper left: face side; upper right: back side) and 21 (lower left face side; lower right back side) at 4.5 Å of the nuclei

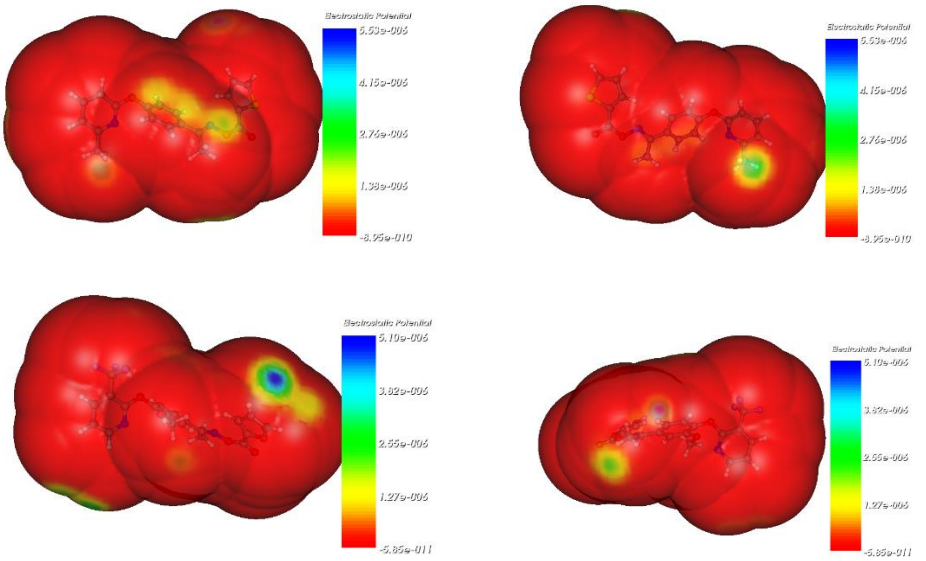

Figure 40: MEP map of molecules 14 (upper left: face side; upper right: back side) and 21 (lower left: face side; lower right: back side) at 3.5 Å of the nuclei

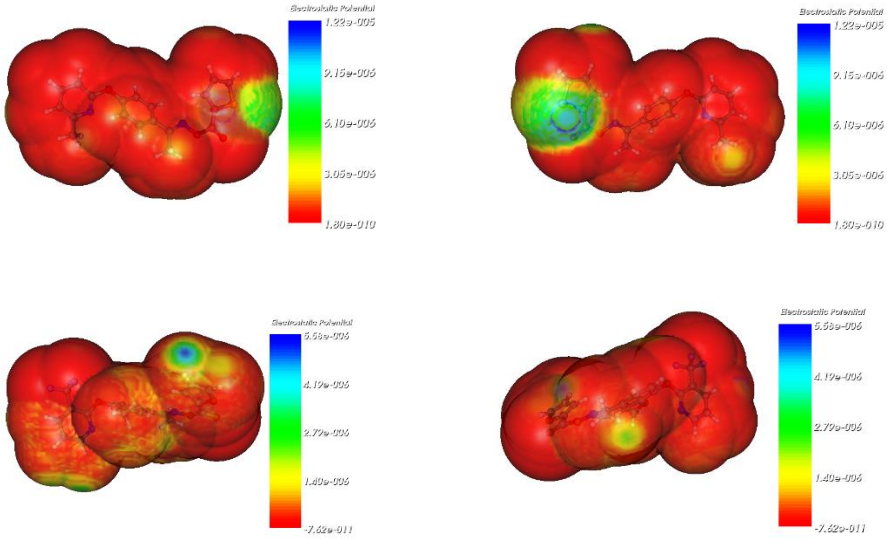

Figure 41: MEP map of molecules 14 (upper left: face side; upper right: back side) and 21 (lower left face side; lower right: backside) at 2 Å of the nuclei

The figures give a good idea of how the MEP changes as it is calculated closer and closer to the nuclei. The information that we lack is about the eventual changes that the conformations of the molecules studied here undergo as they approach the receptor and encounter the various amino acids. It can clearly be stated that in the case of a receptor that is on the surface of the structure that supports it, the interactions will be less complicated than in the case of a receptor that is inside a cavity. The need for the MEP of a molecule to match the MEP of the macromolecule can produce significant conformational changes.

Discussion

Equation 2.

Table 2 shows that the importance of variables in Eq. 2 is S_5^N> F_4(HOMO-2)*> S_{26}^N(LUMO+2)*> S_{28}^E> S_4^N(LUMO+1)*~ F_{29}(LUMO+2)*. A high herbicidal activity is associated with large positive numerical values for S_5^N, a large electron population in the third lowest occupied local MO localized on atom 4, large positive numerical values for S_{26}^N(LUMO+2)*, small negative values for S_{28}^E, small positive numerical values for S_4^N(LUMO+1)* and a small electron population in the third lowest occupied local MO localized on atom 29. Note that all these reactivity indices belong to ring A atoms or to substituents attached to it.

Atom 5 is a sp^2 carbon in ring A (see Fig. 5). A high PPO inhibitory activity is associated with large positive numerical values for S_5^N. From the definition of this reactivity index, we know that the first terms (the first three or four lowest empty MOs) are the dominant ones. Large positive values are obtained by shifting downwards the MO energy. The ideal situation is that molecule's LUMO, (LUMO+1) and (LUMO+2) be localized on this atom. Therefore, atom 5 seems to interact with an electron-rich center. This suggestion is consistent with the fact that atom 5 is bonded to a nitrogen and oxygen atoms. The ideal situation is that the three highest occupied local MOs of atom 5 be of pi nature.

Atom 4 is a sp^2 carbon in ring A (see Fig. 5). Table 4 shows that the first lowest empty local MO, (LUMO)*, coincides with the molecule's molecular orbitals (LUMO+1) or (LUMO+2). The nature of this local MO is π in almost all molecules. A high PPO inhibitory activity is associated with large positive numerical values for S_{26}^N(LUMO+2)*. These values are obtained by shifting downwards the MO energy. The ideal situation would be when the molecular LUMO is localized on this atom. On this basis we suggest that this atom is interacting with an electron-rich center. Figures 42 to 47 show the electronic density of the three lowest empty local MOs of atom 4 of molecules 14 and 21. Also the electron density in the plane defined by atom 1, 2 and 3 is shown.

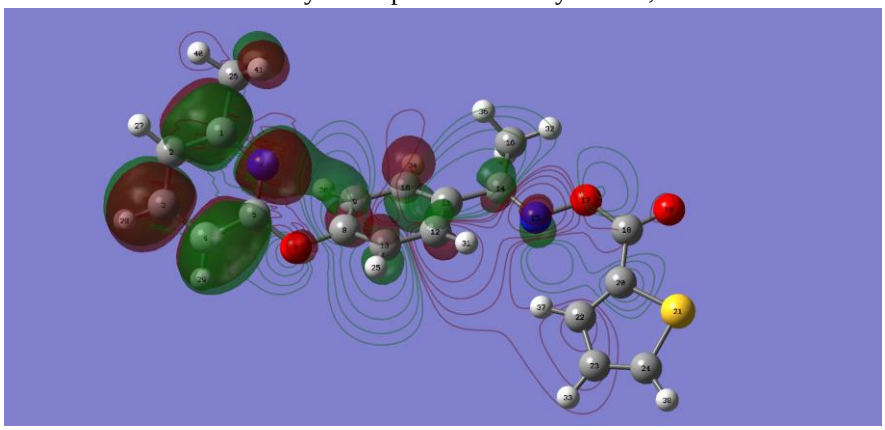

Figure 42: Molecule 14. Local $(LUMO)_4$ of atom 4 (This is molecular MO number 95). The 2D plane for electron density is defined by atoms 1, 2 and 3.*

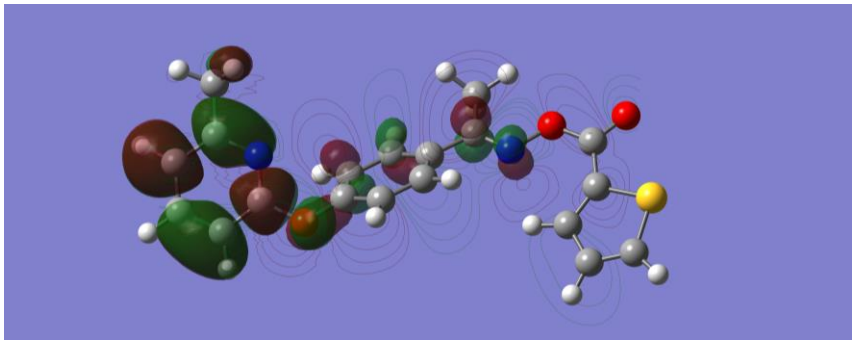

Figure 43: Molecule 14. Local $(LUMO+1)_4$ of atom 4 (This is molecular MO number 97). The 2D plane for electron density is defined by atoms 1, 2 and 3.*

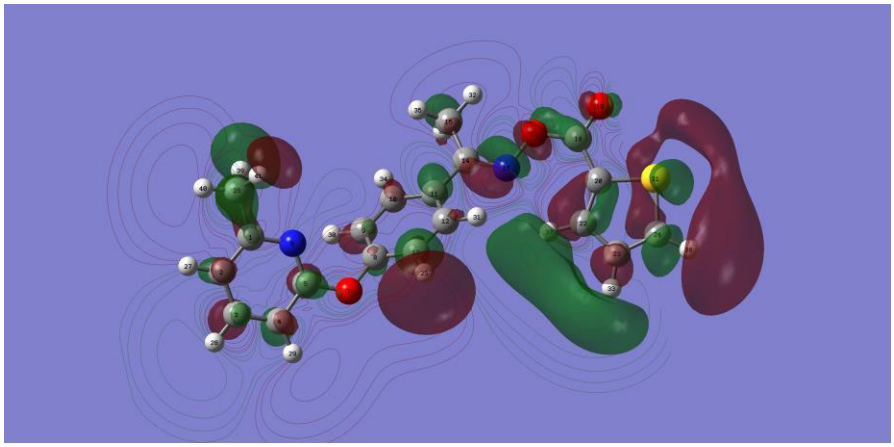

Figure 44: Molecule 14. Local $(LUMO+2)_4$ of atom 4 (This is molecular MO number 111). The 2D plane for electron density is defined by atoms 1, 2 and 3.*

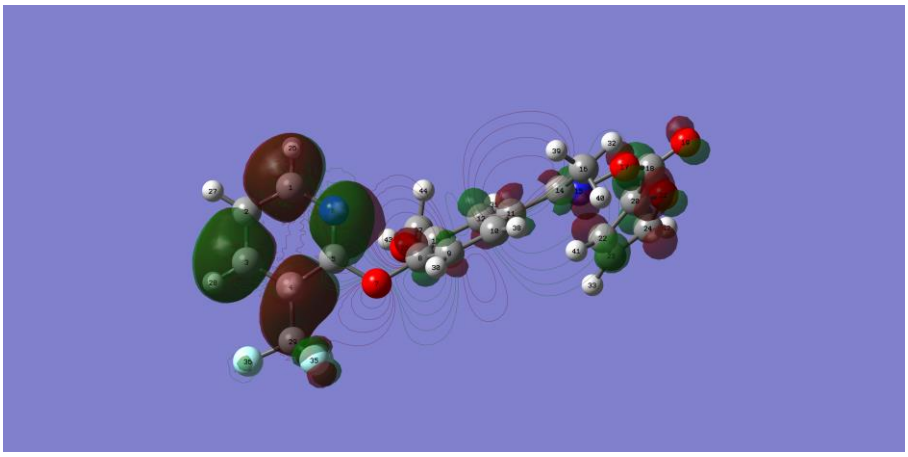

Figure 45: Molecule 21. Local $(LUMO)_4$ of atom 4 (This is molecular MO number 110). The 2D plane for electron density is defined by atoms 1, 2 and 3.*

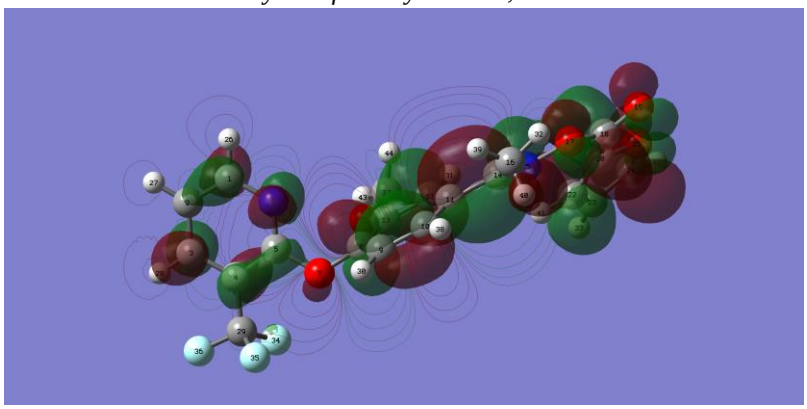

Figure 46: Molecule 21. Local $(LUMO+1)_4$ of atom 4 (This is molecular MO number 111). The 2D plane for electron density is defined by atoms 1, 2 and 3.*

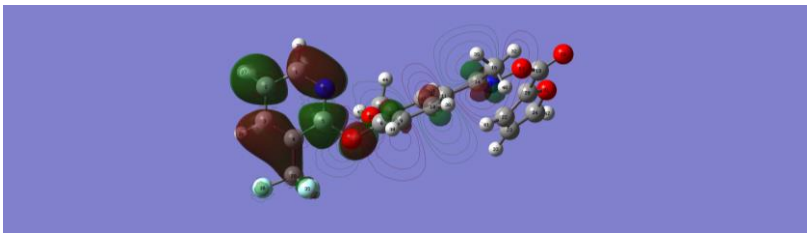

Figure 47: Molecule 21. Local $(LUMO+2)_4$ of atom 4 (This is molecular MO number 112). The 2D plane for electron density is defined by atoms 1, 2 and 3.*

On the other hand, a high inhibitory activity is associated also with a large electron population in the third lowest occupied local MO, $(HOMO-2)_4$*. This local MO has π or σ nature (see Table 4). Theoretically this suggests the interaction with an electron-deficient center. This is contradictory to the previous condition, but one way to solve this issue is to propose that atom 4 interacts with two different sites in the receptor that are in opposite places.

Atom 26 is the substituent's atom directly bonded to C-1 (see Figs. 1 and 5). Table 1 shows that these substituents are: H, Me, NO_2, Br and CF_3. A high PPO inhibitory activity is associated with large positive numerical values for $S_{26}^N(LUMO+2)$*. This suggests that atom 26 should be interacting with an electron-rich center. This case presents us with an interpretation problem in the sense that atom 26 (substituent) may be interacting directly with the receptor site or it is simply accounting for the interaction of one of the atoms attached to it that is not included in the common skeleton. $(LUMO+2)_{26}^*$ has a sigma nature in almost all the molecules (Table 5). Large numerical values for this reactivity index are obtained by shifting downwards the MO energy, making it more reactive. Therefore, the ideal situation is when the molecular LUMO, (LUMO+1) and (LUMO+2) are localized on this atom with the highest possible numerical value for the associated Fukui indices. H, $C(H_3)$, $N(O_2)$, Br and $C(F_3)$ can interact with an electron-rich center but in different ways. Since this issue requires further investigation through the synthesis of new derivatives and some advances in theory, we will not propose any specific type of interaction for the moment.

Atom 28 is the substituent's atom directly bonded to C-3 (see Figs. 1 and 5). Table 1 shows that these substituents are: H, Me, NO_2, Cl and CF_3. A high herbicidal activity is associated with small negative numerical values for S_{28}^E. These values can be obtained by shifting downwards the MO energies of the highest occupied local MOs. This will transform atom 28 in a bad electron donor. This suggests that atom 28 should be interacting with an electron-rich center. For the same reasons invoked in the case of atom 26 we will refrain from suggesting the form of the interactions.

Atom 29 is the substituent's atom directly bonded to C-3 (see Figs. 1 and 5). A high herbicidal activity is associated with a small electron population in the third lowest occupied local MO localized on atom 29, $(LUMO+2)_{29}^*$. Substituents are H and OCH_3. Table 4 shows that all MOs are sigma. The local (LUMO)* coincides with empty molecular MOs that are energetically far from the molecular LUMO. Now we can only suggest that this atom interacts with an electron-rich site. For the same reasons invoked in the case of atom 26 we will refrain from suggesting the form of the interactions. All the suggestions are displayed in the partial 2D pharmacophore of Fig. 48.

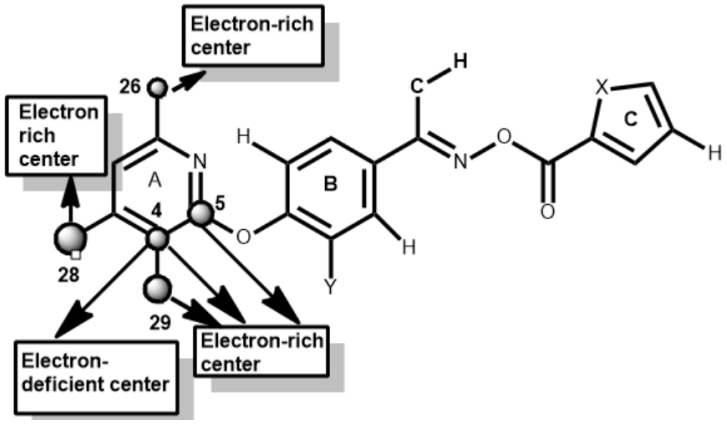

Figure 48: Partial 2D pharmacophore for Eq. 2.

Discussion of Equation 3.

Table 7 shows that the importance of variables in Eq. 3 is F_{28}(LUMO+1)*>> S_6^N(LUMO+1)*> Q_2^{max}. A high herbicidal activity is associated with high numerical values for F_{28}(LUMO+1)*, high numerical positive values for S_6^N(LUMO+1)* and high numerical positive values for Q_2^{max}.

Atom 28 is the atom of the substituent directly bonded to a carbon atom of ring A (see Table 1, Fig. 1, and Fig. 5). High numerical values for F_{28}(LUMO+1)* are required for high herbicidal activity. This suggests that an ideal activity is when $(LUMO+1)_{28}^*$ has a large Fukui index (i.e., the corresponding local MO is highly localized on this atom). This suggests that atom 28 is interacting with an electron-rich center. This suggestion is consistent with the one produced by Equation 2.

Atom 2 is a sp^2 carbon in ring A (Fig. 1 and Fig. 5). Table 10 shows that all frontier local molecular orbitals have a π nature. As high herbicidal activity is associated with high numerical positive values for Q_2^{max}, the ideal situation is when $(LUMO)_2^*$ is highly localized on atom 2 in such a way that if can receive a good amount of charge. This suggests that atom 2 is interacting with an electron-rich center.

Atom 6 is a nitrogen atom in ring A (Fig. 1 and Fig. 5). Table 10 shows that $(HOMO)_2^*$ has a pi or lone pair nature, and that $(LUMO)_2^*$ has a pi nature in all molecules. High numerical positive values for S_6^N(LUMO+1)* are associated with good herbicide activity. This suggests that atom 6 is interacting with an electron-rich center. All the above suggestions are displayed below in the partial 2D pharmacophore of Eqn. 3 and 4.

Discussion of Equation 4.

The only variable in Eq. 4 is S_{14}^E(HOMO)*. Atom 14 is a sp^2 carbon atom located in the chain linking rings B and C. Table 10 shows that the local HOMO* have a pi nature in all molecules. A high herbicidal activity is associated with high numerical negative values for S_{14}^E(HOMO)*. These highly negative values are obtained by shifting upwards the molecular orbital energy, bringing it closer to zero. This will make $(HOMO)_{14}^*$ highly reactive toward an electron-deficient center. Therefore, our suggestion is that atom 14 interacts with such a center. The above suggestions produced by Eq. 3 and 4 are displayed in the partial 2D pharmacophore of Fig. 49.

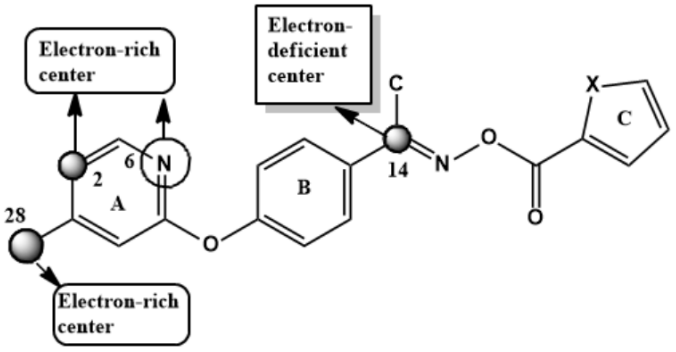

Figure 49: Partial 2D pharmacophore for Eq. 3 and 4

It should be mentioned that the fact that in pharmacophores more than one atom points towards a certain center does not imply that said center is common to those atoms.

In summary, for a series of biphenyl ether derivatives having a five-membered heterocycle we found excellent relationships between electronic structure and herbicidal activity. It is expected that the information provided here could be useful for experimentalists.

The author declares no competing financial interest and states that the research reported here meets the standards of the Singapore Statement on Research Integrity. In this paper artificial intelligence writing tools were not employed.

Lic. Soloaga-Ardiles is thanked for preparing the first set of molecular coordinates and creating the rough copies of the Tables of local molecular orbitals.

References

[1]. Kobayashi, D.; Watanabe, E. *Handbook on herbicides: biological activity, classification and health & environmental implications*. Nova Science Publishers: Hauppauge, N.Y., 2014; p xiii, 317 p.

[2]. Cobb, A. H. *Herbicides and plant physiology*. Third edition. ed.; John Wiley & Sons: Chichester, West Sussex, 2022; p 1 online resource.

[3]. Rangani, G.; Salas-Perez, R. A.; Aponte, R. A.; Knapp, M.; Craig, I. R.; Mietzner, T.; Langaro, A. C.; Noguera, M. M.; Porri, A.; Roma-Burgos, N. A Novel Single-Site Mutation in the Catalytic Domain of Protoporphyrinogen Oxidase IX (PPO) Confers Resistance to PPO-Inhibiting Herbicides. *Frontiers in Plant Science* **2019,** 10.

[4]. Zhao, L.-X.; Peng, J.-F.; Liu, F.-Y.; Zou, Y.-L.; Gao, S.; Fu, Y.; Ye, F. Design, synthesis, and herbicidal activity of diphenyl ether derivatives containing a five-membered heterocycle. *Journal of Agricultural and Food Chemistry* **2022,** 70, 1003-1018.

[5]. Price, A.; Kelton, J.; Sarunaite, L. *Herbicides: Physiology of Action and Safety*. AvE4EvA: N/A, 2015.

[6]. Liu, H.-Y.; Yu, L.-K.; Qin, S.-N.; Yang, H.-Z.; Wang, D.-W.; Xi, Z. Design, Synthesis, and Metabolism Studies of N-1, 4-Diketophenyltriazinones as Protoporphyrinogen IX Oxidase Inhibitors. *Journal of Agricultural and Food Chemistry* **2023**.

[7]. Zhao, L.-x.; Peng, J.-f.; Liu, F.-y.; Zou, Y.-l.; Gao, S.; Fu, Y.; Ye, F. Discovery of novel phenoxypyridine as promising protoporphyrinogen IX oxidase inhibitors. *Pesticide Biochemistry and Physiology* **2022,** 184, 105102.

[8]. Liang, L.; Yu, S.; Li, Q.; Wang, X.; Wang, D.; Xi, Z. Design, synthesis, and molecular simulation studies of N-phenyltetrahydroquinazolinones as protoporphyrinogen IX oxidase inhibitors. *Bioorganic & Medicinal Chemistry* **2021,** 39, 116165.

[9]. Zhang, R.-B.; Yu, S.-Y.; Liang, L.; Ismail, I.; Wang, D.-W.; Li, Y.-H.; Xu, H.; Wen, X.; Xi, Z. Design, synthesis, and molecular mechanism studies of N-phenylisoxazoline-thiadiazolo [3, 4-a] pyridazine hybrids as protoporphyrinogen IX oxidase inhibitors. *Journal of Agricultural and Food Chemistry* **2020,** 68, 13672-13684.

[10]. Lee, W. H.; Kwon, Y. B.; Kim, J. H.; Lee, K. H.; Maezono, S. M. B.; Choi, J.-S.; Seu, Y.-B. Design and synthesis of acrylate and acrylamide substituted pyrimidinediones as potential PPO herbicides. *Bioorganic & Medicinal Chemistry* **2021,** 31, 115959.

[11]. Zhao, L.-X.; Jiang, M.-J.; Hu, J.-J.; Zou, Y.-L.; Gao, S.; Fu, Y.; Ye, F. Herbicidal activity and molecular docking study of novel PPO inhibitors. *Weed Science* **2020,** 68, 565-574.

[12]. Selby, T. P.; Ruggiero, M.; Hong, W.; Travis, D. A.; Satterfield, A. D.; Ding, A. X. Broad-spectrum PPO-inhibiting N-phenoxyphenyluracil acetal ester herbicides. In *Discovery and Synthesis of Crop Protection Products*, ACS Publications: New York, 2015; pp 277-289.

[13]. Zhao, L.-x.; Hu, J.-j.; Wang, Z.-x.; Yin, M.-l.; Zou, Y.-l.; Gao, S.; Fu, Y.; Ye, F. Novel phenoxy-(trifluoromethyl) pyridine-2-pyrrolidinone-based inhibitors of protoporphyrinogen oxidase: Design, synthesis, and herbicidal activity. *Pesticide Biochemistry and Physiology* **2020,** 170, 104684.

[14]. Gao, W.; Li, X.; Ren, D.; Sun, S.; Huo, J.; Wang, Y.; Chen, L.; Zhang, J. Design and synthesis of N-phenyl phthalimides as potent protoporphyrinogen oxidase inhibitors. *Molecules* **2019,** 24, 4363.

[15]. Wang, D.-W.; Li, Q.; Wen, K.; Ismail, I.; Liu, D.-D.; Niu, C.-W.; Wen, X.; Yang, G.-F.; Xi, Z. Synthesis and herbicidal activity of pyrido [2, 3-d] pyrimidine-2, 4-dione–benzoxazinone hybrids as protoporphyrinogen oxidase inhibitors. *Journal of Agricultural and Food Chemistry* **2017,** 65, 5278-5286.

[16]. Zuo, Y.; Wu, Q.; Su, S.-w.; Niu, C.-w.; Xi, Z.; Yang, G.-F. Synthesis, herbicidal activity, and QSAR of novel N-benzothiazolyl-pyrimidine-2, 4-diones as protoporphyrinogen oxidase inhibitors. *Journal of Agricultural and Food Chemistry* **2016,** 64, 552-562.

[17]. Jiang, L.-L.; Tan, Y.; Zhu, X.-L.; Wang, Z.-F.; Zuo, Y.; Chen, Q.; Xi, Z.; Yang, G.-F. Design, synthesis, and 3D-QSAR analysis of novel 1, 3, 4-oxadiazol-2 (3 H)-ones as protoporphyrinogen oxidase inhibitors. *Journal of Agricultural and Food Chemistry* **2010,** 58, 2643-2651.

[18]. The results presented here are obtained from what is now a routinary procedure. For this reason, all papers have a similar general structure. This model contains *standard* phrases for the presentation of the methods, calculations and results because they do not need to be rewritten repeatedly and because the number of possible variations to use is finite. See: Hall, S., Moskovitz, C., and Pemberton, M. 2021. Understanding Text Recycling: A Guide for Researchers. Text Recycling Research Project. Online at textrecycling.org. In.

[19]. Gómez Jeria, J. S. La Pharmacologie Quantique. *Bollettino Chimico Farmaceutico* **1982,** 121, 619-625.

[20]. Gómez-Jeria, J. S. On some problems in quantum pharmacology I. The partition functions. *International Journal of Quantum Chemistry* **1983,** 23, 1969-1972.
[21]. Gómez-Jeria, J. S. Modeling the Drug-Receptor Interaction in Quantum Pharmacology. In *Molecules in Physics, Chemistry, and Biology*, Maruani, J., Ed. Springer Netherlands: 1989; Vol. 4, pp 215-231.
[22]. Gómez-Jeria, J. S.; Ojeda-Vergara, M. Parametrization of the orientational effects in the drug-receptor interaction. *Journal of the Chilean Chemical Society* **2003,** 48, 119-124.
[23]. Gómez-Jeria, J. S. *Elements of Molecular Electronic Pharmacology (in Spanish)*. 1st ed.; Ediciones Sokar: Santiago de Chile, 2013; p 104.
[24]. Gómez-Jeria, J. S. A New Set of Local Reactivity Indices within the Hartree-Fock-Roothaan and Density Functional Theory Frameworks. *Canadian Chemical Transactions* **2013,** 1, 25-55.
[25]. Gómez-Jeria, J. S.; Espinoza, L. Quantum-chemical studies on acetylcholinesterasa inhibition. I. Carbamates. *Journal of the Chilean Chemical Society* **1982,** 27, 142-144.
[26]. Gómez-Jeria, J. S.; Morales-Lagos, D. The mode of binding of phenylalkylamines to the Serotonergic Receptor. In *QSAR in design of Bioactive Drugs*, Kuchar, M., Ed. Prous, J.R.: Barcelona, Spain, 1984; pp 145-173.
[27]. Gómez-Jeria, J. S.; Morales-Lagos, D.; Rodriguez-Gatica, J. I.; Saavedra-Aguilar, J. C. Quantum-chemical study of the relation between electronic structure and pA2 in a series of 5-substituted tryptamines. *International Journal of Quantum Chemistry* **1985,** 28, 421-428.
[28]. Gómez-Jeria, J. S.; Sotomayor, P. Quantum chemical study of electronic structure and receptor binding in opiates. *Journal of Molecular Structure: THEOCHEM* **1988,** 166, 493-498.
[29]. Gómez-Jeria, J. S.; Ojeda-Vergara, M.; Donoso-Espinoza, C. Quantum-chemical Structure-Activity Relationships in carbamate insecticides. *Molecular Engineering* **1995,** 5, 391-401.
[30]. Gómez-Jeria, J. S.; Lagos-Arancibia, L.; Sobarzo-Sánchez, E. Theoretical study of the opioid receptor selectivity of some 7-arylidenenaltrexones. *Boletin de la Sociedad Chilena de Quimica* **2003,** 48, 61-66.
[31]. Gómez-Jeria, J. S.; Gerli-Candia, L. A.; Hurtado, S. M. A structure-affinity study of the opioid binding of some 3-substituted morphinans. *Journal of the Chilean Chemical Society* **2004,** 49, 307-312.
[32]. Soto-Morales, F.; Gómez-Jeria, J. S. A theoretical study of the inhibition of wild-type and drug-resistant HTV-1 reverse transcriptase by some thiazolidenebenzenesulfonamide derivatives. *Journal of the Chilean Chemical Society* **2007,** 52, 1214-1219.
[33]. Barahona-Urbina, C.; Nuñez-Gonzalez, S.; Gómez-Jeria, J. S. Model-based quantum-chemical study of the uptake of some polychlorinated pollutant compounds by Zucchini subspecies. *Journal of the Chilean Chemical Society* **2012,** 57, 1497-1503.
[34]. Bruna-Larenas, T.; Gómez-Jeria, J. S. A DFT and Semiempirical Model-Based Study of Opioid Receptor Affinity and Selectivity in a Group of Molecules with a Morphine Structural Core. *International Journal of Medicinal Chemistry* **2012,** 2012 Article ID 682495, 1-16.
[35]. Alarcón, D. A.; Gatica-Díaz, F.; Gómez-Jeria, J. S. Modeling the relationships between molecular structure and inhibition of virus-induced cytopathic efects. Anti-HIV and anti-H1N1 (Influenza) activities as examples. *Journal of the Chilean Chemical Society* **2013,** 58, 1651-1659.
[36]. Muñoz-Gacitúa, D.; Gómez-Jeria, J. S. Quantum-chemical study of the relationships between electronic structure and anti influenza activity. 1. The inhibition of cytophatic effects produced by the influenza A/Guangdong Luohu/219/2006 (H1N1) strain in MDCK cells by substituted bisaryl amide compounds. *Journal of Computational Methods in Molecular Design* **2014,** 4, 33-47.
[37]. Muñoz-Gacitúa, D.; Gómez-Jeria, J. S. Quantum-chemical study of the relationships between electronic structure and anti influenza activity. 2. The inhibition by 1H-1,2,3-triazole-4-carboxamide derivatives of the cytopathic effects produced by the influenza A/WSN/33 (H1N1) and A/HK/8/68 (H3N2) strains in MDCK cells. *Journal of Computational Methods in Molecular Design* **2014,** 4, 48-63.
[38]. Gómez-Jeria, J. S.; Robles-Navarro, A. A Density Functional Theory and Docking study of the Relationships between Electronic Structure and 5-HT_{2B} Receptor Binding Affinity in N-Benzyl Phenethylamines. *Der Pharma Chemica* **2015,** 7, 243-269.
[39]. Gómez-Jeria, J. S.; Robles-Navarro, A. Quantum-chemical study of the cytotoxic activity of pyrimidine–benzimidazol hybrids against MCF-7, MGC-803, EC-9706 and SMMC-7721 human cancer cell lines. *Research Journal of Pharmaceutical, Biological and Chemical Sciences* **2015,** 6, 755-783.
[40]. Gómez-Jeria, J. S.; Valdebenito-Gamboa, J. Electronic structure and docking studies of the Dopamine D_3 receptor binding affinity of a series of [4-(4-Carboxamidobutyl)]-1-arylpiperazines. *Der Pharma Chemica* **2015,** 7, 323-347.

[41]. Gómez-Jeria, J. S.; Garrido-Sáez, N. A DFT analysis of the relationships between electronic structure and affinity for dopamine D_2, D_3 and D_4 receptor subtypes in a group of 77-LH-28-1 derivatives. *Chemistry Research Journal* **2019,** 4, 30-42.
[42]. Gómez-Jeria, J. S.; Gatica-Díaz, N. A preliminary quantum chemical analysis of the relationships between electronic structure and 5-HT_{1A} and 5-HT_{2A} receptor affinity in a series of 8-acetyl-7-hydroxy-4-methylcoumarin derivatives. *Chemistry Research Journal* **2019,** 4, 85-100.
[43]. Gómez-Jeria, J. S.; Sánchez-Jara, B. An introductory theoretical investigation of the relationships between electronic structure and A1, A2A and A3 adenosine receptor affinities of a series of N6-8,9-trisubstituted purine derivatives. *Chemistry Research Journal* **2019,** 4, 46-59.
[44]. Gómez-Jeria, J. S.; González-Ponce, N. A Quantum-chemical study of the relationships between electronic structure and affinities for the serotonin transporter protein and the 5-HT_{1A} receptor in a series of 2H-pyrido[1,2-c]pyrimidine derivatives. *Chemistry Research Journal* **2020,** 5, 16-31.
[45]. Gómez-Jeria, J. S.; Rojas-Candia, V. A DFT Investigation of the Relationships between Electronic Structure and D_2, 5-HT_{1A}, 5-HT_{2A}, 5-HT_6 and 5-HT_7 Receptor Affinities in a group of Fananserin derivatives. *Chemistry Research Journal* **2020,** 5, 37-58.
[46]. Gómez-Jeria, J. S.; Soloaga Ardiles, C. E.; Kpotin, G. A. A DFT Analysis of the Relationships between Electronic Structure and Human κ, δ and μ Opioid Receptor Binding Affinity in a series of Diphenethylamines. *Chemistry Research Journal* **2020,** 5, 32-46.
[47]. Gómez-Jeria, J. S.; Robles-Navarro, A.; Soza-Cornejo, C. A note on the relationships between electronic structure and serotonin 5-HT_{1A} receptor binding affinity in a series of 4-butyl-arylpiperazine-3-(1*H*-indol-3-yl)pyrrolidine-2,5-dione derivatives. *Chemistry Research Journal* **2021,** 6, 76-88.
[48]. Gómez-Jeria, J. S.; Ibertti-Arancibia, A.; Olarte-Lezcano, L. A theoretical study of the relationships between electronic structure of 2-aryladenine derivatives and percentage of inhibition of radioligand binding in human A_{2A} and A_{2B} adenosine receptors. *Chemistry Research Journal* **2022,** 7, 1-18.
[49]. Gómez-Jeria, J. S.; Olarte-Lezcano, L. On the relationships between electronic structure and 5-HT_{2A}, 5-HT_{2C} and D_2 receptor affinities in a group of 2-aryl tryptamines. A DFT study. *Chemistry Research Journal* **2022,** 7, 14-35.
[50]. Gómez-Jeria, J. S.; Pinto-Saldaña, M. Electronic structure and D_2, 5-HT_{1A}, 5-HT_{2A} and H_3 receptor affinities of some multi-target heterocycle piperazine derivatives. A DFT and FQSAR study. *Chemistry Research Journal* **2022,** 7, 52-83.
[51]. Frisch, M. J.; Trucks, G. W.; Schlegel, H. B.; Scuseria, G. E.; Robb, M. A.; Cheeseman, J. R.; Scalmani, G.; Barone, V.; Petersson, G. A.; Nakatsuji, H.; Li, X.; Caricato, M.; Marenich, A. V.; Bloino, J.; Janesko, B. G.; Gomperts, R.; Mennucci, B.; Hratchian, H. P. *Gaussian 16 16Rev. A.03*, Gaussian: Pittsburgh, PA, USA, 2016.
[52]. Gómez-Jeria, J. S. *D-Cent-QSAR: A program to generate Local Atomic Reactivity Indices from Gaussian16 log files*, v. 1.0; Santiago, Chile, 2020.
[53]. Gómez-Jeria, J. S. An empirical way to correct some drawbacks of Mulliken Population Analysis (Erratum in: J. Chil. Chem. Soc., 55, 4, IX, 2010). *Journal of the Chilean Chemical Society* **2009,** 54, 482-485.
[54]. Statsoft. *Statistica v. 8.0*, 2300 East 14 th St. Tulsa, OK 74104, USA, 1984-2007.
[55]. Gómez-Jeria, J. S.; Robles-Navarro, A.; Kpotin, G.; Garrido-Sáez, N.; Gatica-Díaz, N. Some remarks about the relationships between the common skeleton concept within the Klopman-Peradejordi-Gómez QSAR method and the weak molecule-site interactions. *Chemistry Research Journal* **2020,** 5, 32-52.
[56]. Hypercube. *Hyperchem 7.01*, 7.01; 419 Phillip St., Waterloo, Ontario, Canada, 2002.
[57]. Chemaxon. *MarvinView*, 23.1.0; www.chemaxon.com: USA, 2023.
[58]. Systèmes, D. *BIOVIA Discovery Studio Visualizer v. 20.1*, San Diego: Dassault Systèmes, 2019.
[59]. Dennington, R. D.; Keith, T. A.; Millam, J. M. *GaussViev 5.0.8*, GaussViev 5.0.8, 340 Quinnipiac St., Bldg. 40, Wallingford, CT 06492, USA, 2000-2008.
[60]. Varetto, U. *Molekel 5.4.0.8*, Swiss National Supercomputing Centre: Lugano, Switzerland, 2008.